UNIVERSITY OF CRETE
DEPARTMENT OF PHYSICS

FOUNDATION FOR RESEARCH AND TECHNOLOGY HELLAS INSTITUTE OF ELECTRONIC STRUCTURE AND LASER

BACHELOR THESIS

<<Development of composite 2D material-glasses (MoS_2-glasses) for optoelectronics applications>>

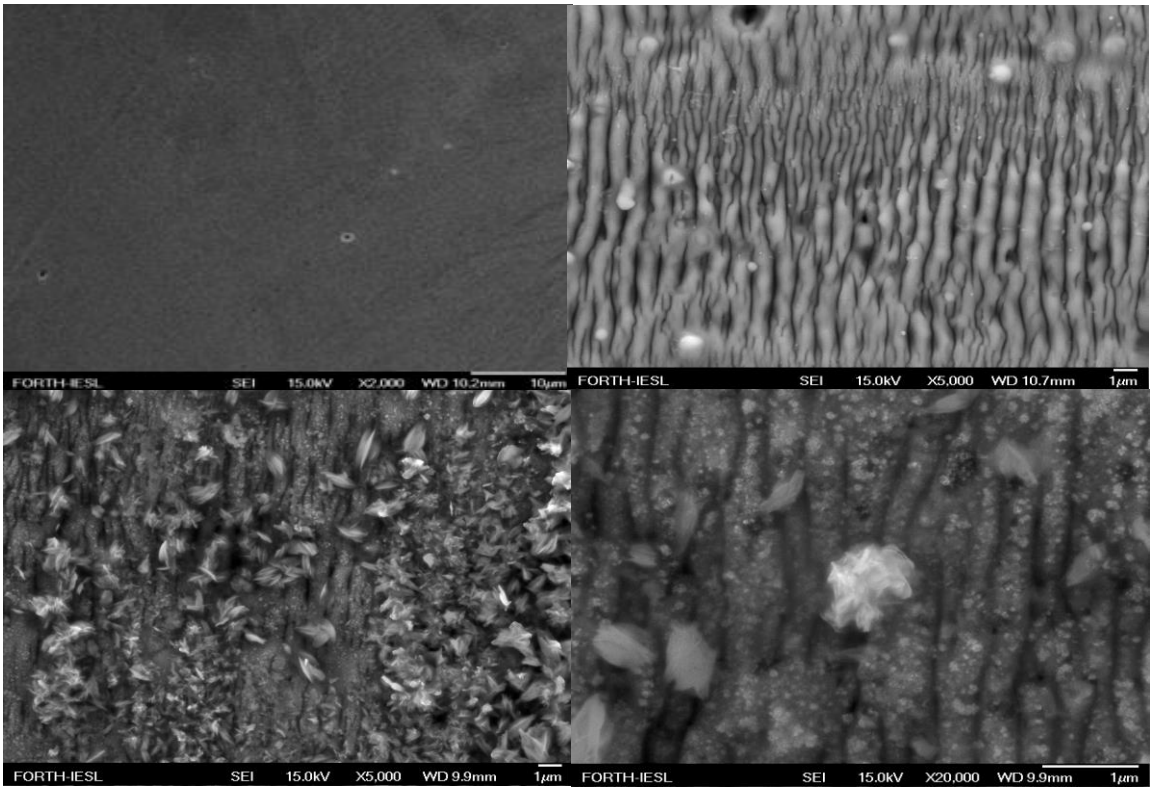

HARRIS GONIOTAKIS

Supervisors: Dr. Emmanuel Stratakis, Dr. Ioannis Konidakis

ΕΥΧΑΡΙΣΤΙΕΣ

Η ολοκλήρωση της πτυχιακής μου εργασίας, δεν θα γινόταν εφικτή χωρίς την καθοριστική συμβολή και καθοδήγηση κάποιων ανθρώπων, τους οποίους θα ήθελα να τους ευχαριστήσω προσωπικά. Τον Δρ. Εμμανουήλ Στρατάκη, ερευνητικός διευθυντής στο Ινστιτούτο Ηλεκτρονικής δομής και Laser του Ιδρύματος Τεχνολογίας και Έρευνας-FORTH και Leader της ερευνιτικής ομάδας ULMNP (Ultrafast Laser Micro- and Nano- Processing) για την δυνατότητα που μου έδωσε να εκπαιδευτώ και να μάθω πολλά πράγματα στο εργαστήριό του. Τον Δρ. Ιωάννη Κονιδάκη, μεταδιδακτορικός ερευνητής της ιδιας ομάδας για την υπομονή, συνεργασία και στήριξη του καθ'όλη την διάρκεια της εργασίας μου, αλλά και για τις πολύτιμες γνώσεις και καθοδήγηση για την ολοκλήρωση της. Τον Δρ. Κωνσταντίνο Τσιμβρακίδη,για την καθοριστική συμβολή του στη δημιουργία των περιοδικών δομών (LIPSS) με χρήση femtosecond laser. Τον Δρ. Abdus S. Sarkar, για την βοήθεια του στην λήψη φασμάτων Raman, και για την βοήθειά του στην παραγωγή few-layered MoS_2 μέσω της μεθόδου Liquid Phase Exfoliation (LPE). Την υπόλοιπη ομάδα του ULMNP, για το άριστο κλίμα της συνεργασίας μας καθώς και για όλη βοήθεια που μου προσέφεραν. Την Δρ. Ιωάννα Δεμερίδου, για την λήψη φασμάτων Photoluminescence. Και φυσικά, την κα. Αλέκα Μανουσάκη, τεχνικός του ηλεκτρονικού μικροσκοπίου σάρωσης (SEM), για την υπερπολύτιμη βοήθεια στην ανάλυση φωτογραφιών αμέτρητων δειγμάτων, αλλά και στην ανάλυση του προφιλόμετρου για τα δείγματα αυτά. Επίσης, θα ήθελα να ευχαριστήσω τον καθηγητή μου κ. Γιώργο Κοκκινίδη ο οποίος με βοήθησε να ανακαλύψω το ενδιαφέρον μου για την Φυσική από όταν ήμουν μικρός, και έπαιξε σημαντικό ρόλο στο να επιτύχω τον στόχο μου να σπουδάσω την επιστήμη που μου αρέσει. Τέλος, θέλω να πω ένα μεγάλο ευχαριστώ στην οικογένειά μου, για την στηρίξη που μου παρείχε όλα τα χρόνια των σπουδών μου, ώστε να ολοκληρώσω με επιτυχία το πτυχίο μου.

Contents

Abstract

Transition metal dichalcogenides (TMDs) are semiconductors consisting of a transition metal and two chalcogen atoms. They have a chemical type of MX_2 where M is a transition metal and X a chalcogen atom. They are part of a larger group known as 2D materials named so to emphasize their extraordinary thickness, which is at the order of some Å. In their monolayer form, TMDs have a direct bandgap and this makes them ideal for their use in various applications in valleytronics, electronics (as transistors) and in optics (as photoemitters and detectors). Therefore, monolayer TMDs have received significant attention. Monolayer Molybdenum disulfide (MoS_2) in particular, gains considerable attention due to its direct band gap and potential integration with other nanostructures to form nanoscale van der Waals heterojunctions with intriguing physical and optical properties. Indeed, several studies have been carried out for an attempt to enhance and control the optical properties of the monolayer (mostly) and few layers MoS_2. For example, Catalan-Gomez et al. used MoS_2 monolayers and Ga nanoparticles (NPs) in a attempt to enhance the photoluminescence (PL) of the 2D material, J.Yan et al. used few-layered MoS_2 and Au NPs with the aim of controlling the PL of MoS_2 by controlling the size and aggregation of the Au NPs in various spots, X. Zhang et al. used MoS_2 monolayers and photonic crystals in an attempt to also enhance the PL of MoS_2 and J. Huang et al. utilized silver nanotubes on monolayer MoS_2 to control the A and B exciton emissions. A major breakthrough achieved by Abdus S. Sarkar et al. at ULMNP labs at FORTH, when they embedded few-layered MoS_2 flakes into a sliver metaphosphate ($AgPO_3$) glass matrix. Indeed, they achieved a remarkable enhancement of both A and B exciton emissions at room temperature. It has been also demonstrated by the same group at ULMNP the ability to create laser induced periodic surface structures (LIPSS) on a $AgPO_3$ matrix. It is well known that the excitons in TMDs can interact with plasmonic profiles of metal NPs of various dimensionalities and this can increase the PL of a material. It is also known that when strain is applied on a material, I can change the internal band structure of that material and this has an effect on its optical properties.

The aim of this project is to shed light on how the PL properties of few-layered MoS_2 would change when a plasmon-exciton coupling is combined with a strain profile applied on the 2D material using LIPSS.

Chapter 1: Introduction to Physics Principles

1.1 Semiconductors

A semiconductor can be considered a material having a conductivity ranging between that of an insulator and a metal. The two most important bands within the solid's energy structure are known as Valence and Conduction band. They are the closest to the Fermi level of the energy structure. The main difference between the valence band and conduction band is that valence band specifies the energy level of electrons present in the valence shell of an atomic structure. As against a conduction band holds those electrons that are responsible for conduction[1]. A crucial property of semiconductors is the bandgap; a range of forbidden energies within the electronic structure of the material[2], it can also be considered as the energy difference between the conduction and valence band. Semiconductors typically have bandgap ranging between 1 and 4 eV, whilst insulators have larger bandgaps, often greater than 5 eV. A typical image of a bandgap can be seen in Figure 1.

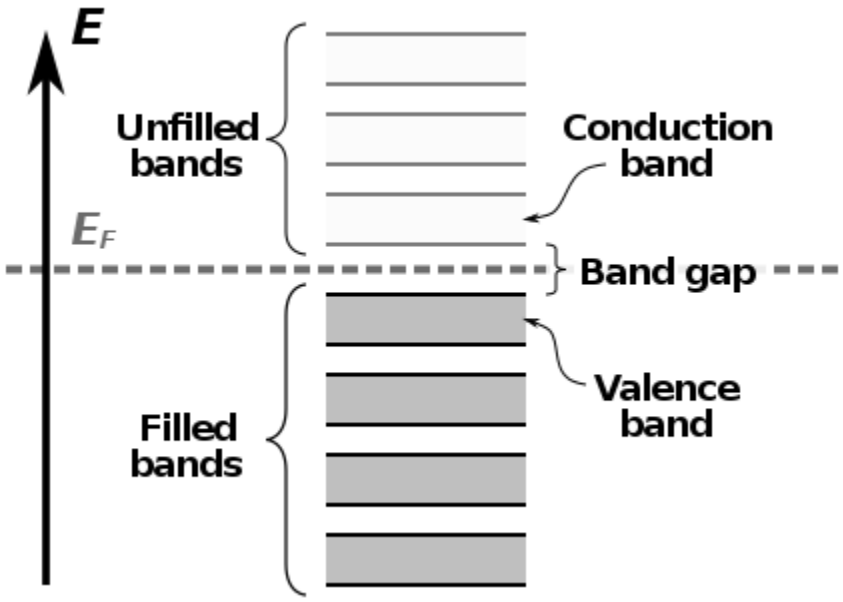

Figure 1: A typical semiconductor energy structure [3].

Depending on the type of bandgap a semiconductor has, they are divided on two categories: a) Direct bandgap semiconductors and b) Indirect bandgap semiconductors. The major difference between those two, is that the lowest point of the conduction band and the highest point of the valence band is at a different point in the reciprocal space (also known as K-Space). So, in order for an electron to be excited from the valence band to the conduction band, it needs not only the energy from a photon, but it also has to change its momentum, which usually happens with a

help of a phonon. The same principle is applied as the electron lowers its energy and drops from the conduction to the valence band. This mechanism is schematically illustrated in Figure 2.

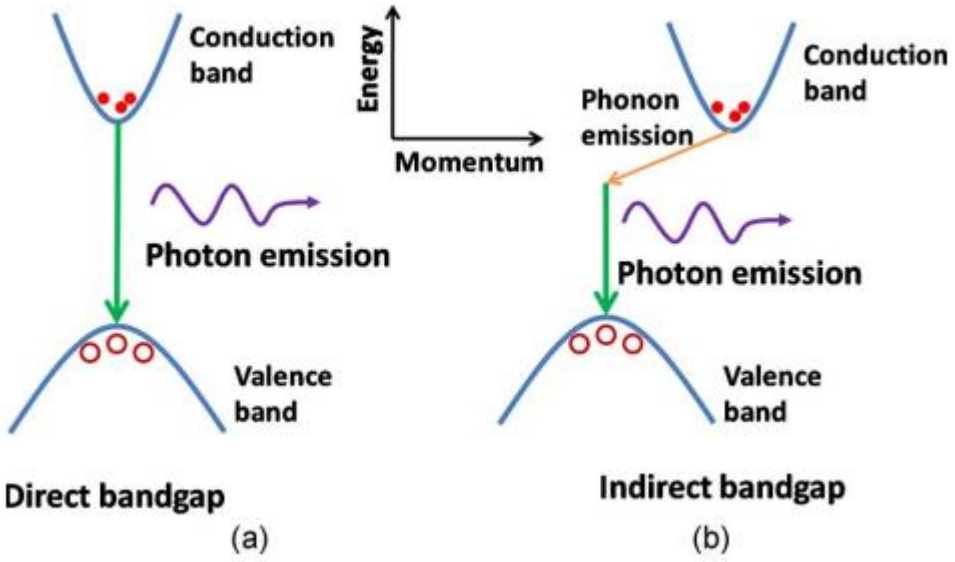

Figure 2: Electron energy transition mechanism in a) Direct and b) Indirect bandgap semiconductor[4].

1.2 Transition Metal Dichalcogenides

The ability to obtain single-layer graphene[5,6] opened up new possibilities and research into the physics of two-dimensional materials. The availability of advanced equipment and tools and a growing understanding of atomically thick layered materials have led to a burgeoning research interest into a whole new range of 2D materials such as transition metal dichalcogenides (TMDs). TMDs are semiconductors of MX_2-type compounds where M is a transition element from groups IV, V, and VI of the periodic table and X represents the chalcogen species S, Se, and Te. Among all TMDs, MoS_2 exhibit superior optoelectronic and catalytic properties compared to the conventional semiconductors[7]. Thus, two-dimensional (2D) TMDs provide an appealing platform for emerging atomic scale research in nanophotonic and optoelectronic applications[8].

Monolayer MoS_2, in particular, gains considerable attention due to its direct band gap and potential integration with other nanostructures to form nanoscale van der Waals heterojunctions with intriguing physical and optical properties. Indeed, it has been shown that the optical properties of MoS_2 monolayers, such as photoluminescence (PL), can be manipulated through its coupling with nanomaterials of various dimensionalities. In particular, zero-dimensional (0D) quantum dots and nanoparticles, one-dimensional (1D) nanowires and nanorods, as well as other 2D materials, had been combined with monolayer MoS_2 to manipulate its emission intensity and/or quantum yield. Besides this, polymeric spacing, defect engineering, doping, and chemical modification approaches were employed to manipulate the emission properties. However,

monolayer MoS_2 suffers from low intrinsic photoluminescence (PL) quantum yield (0.01–0.6%), due to its sub nanometer thickness and defect density mediated nonradiated recombination. The low PL yield was overcome (more than 95%) with chemical treatment by an organic superacid. In contrast to a monolayer MoS_2, few layers of MoS_2 have several orders of magnitude lower PL quantum yield. On the other hand, few-layers MoS_2, as an indirect semiconductor, have significantly larger optical density, which enhances its external quantum efficiency. Owing to this advantage, research on the PL properties in few layers MoS_2 has received significant attention[9].

1.2.1 Structure

TMDs exist in several structural phases resulting from different coordination spheres of the transition metal atoms. The two common structural phases are characterized by either trigonal prismatic (2H) or octahedral (1T) coordination of metal atoms (Figure 3). These structural phases can also be viewed in terms of different stacking orders of the three atomic planes (chalcogen–metal–chalcogen) forming the individual layers of these materials. The 2H phases correspond to an A-B-A stacking in which chalcogen atoms in different atomic planes occupy the same position A and are located on top of each other in the direction perpendicular to the layer. By contrast, the 1T phases are characterized by an ABC stacking order. Depending on the particular combination of transition metal (group IV, V, VI, VII, IX or X) and chalcogen (S, Se or Te) elements, the thermodynamically stable phase is either the 2H or 1T phase, but the other can often be obtained as a metastable phase[10].

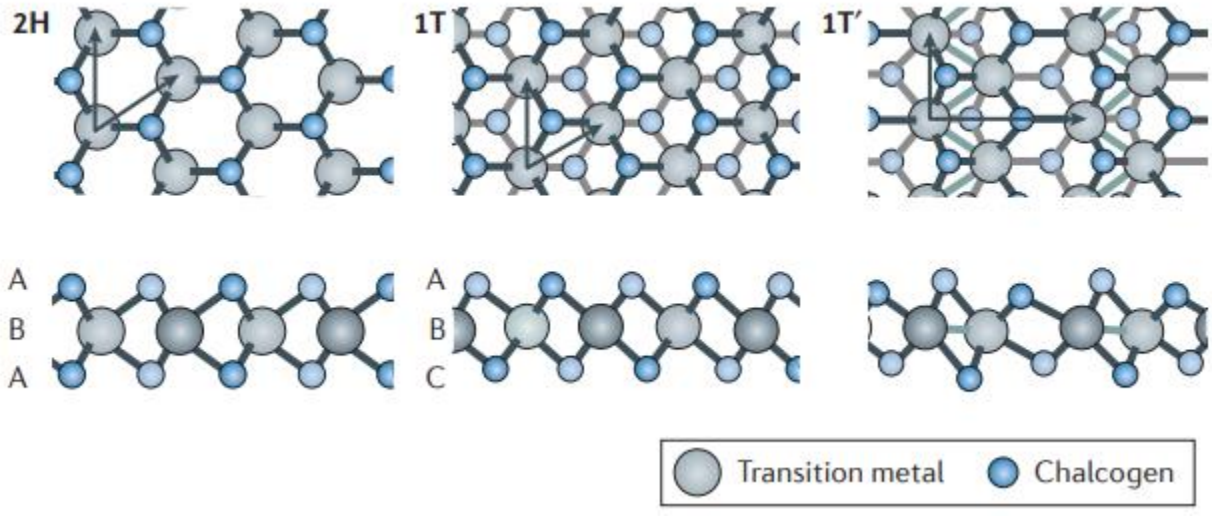

Figure 3: Atomic structure of single layers of transition metal dichalcogenides in their trigonal prismatic (2H), distorted octahedral (1T) and dimerized (1T‘) phases. Lattice vectors and the stacking of atomic planes are indicated[10].

1.2.2 Electronic band structure

The diversity of chemical compositions and structural phases of TMDs results in a broad range of electronic properties, both from the point of view of the band structure character (metallic or insulating) and of the emergence of correlated and topological phases. Here, the basic features of the band structure of TMDCs formed by group VI transition metals Mo and W combined with S and Se are being mentioned.

In their thermodynamically stable 2H phase, MoS_2, $MoSe_2$, WS_2 and WSe_2 are semiconductors. This property drew attention to these TMDs as 2D materials for electronic devices[11]. The evolution of the band structure of 2H-MoS_2 as calculated from first principles[12] (density functional theory) upon reducing its thickness from bulk to monolayer is shown in Figure 4.

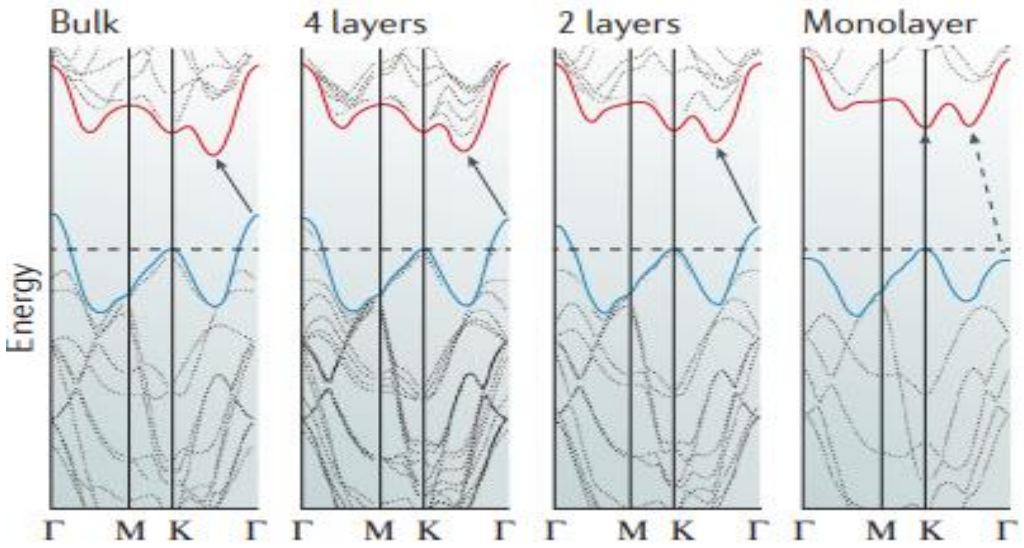

Figure 4: Evolution of the band structure of 2H-MoS_2 calculated for samples of decreasing thickness[10]

As shown, the positions of the valence and conduction band edges change with decreasing thickness, and the indirect bandgap semiconductor bulk material turns into a direct bandgap semiconductor monolayer[8,12]. The calculated values for the bandgap of bulk and monolayer 2H-MoS_2 are 0.88 and 1.71 eV, respectively[13]. The experimental value for the bandgap of monolayer 2H-MoS_2 is 2.16 eV (Ref. 12). Importantly, the valence band maximum and the conduction band minimum are located at the two inequivalent high-symmetry points K and K', which correspond to the corners of the hexagonal Brillouin zone. This property is common to monolayer 2H-MoS_2 (and other group VI monolayer 2H-TMDs), and enables the observation of valley-dependent physical phenomena and potential valleytronics applications.

Another important peculiarity of monolayer 2H-TMDs, is that they lack inversion symmetry, which results in a spin splitting of the electronic bands driven by the spin–orbit interaction. Because points K and K' do not correspond to the time-reversal invariant momenta, the spin degeneracy of the conduction and valence band extrema at these points is lifted. This effect is particularly strong in the valence band, in which spin splitting values range from 0.15 eV in monolayer 2H-MoS_2 to 0.46 eV in 2H-WSe_2 [14]. This trend is understood by considering that the spin–orbit interaction is a relativistic effect, and hence is stronger for heavier elements. Even though the spin splitting of the conduction band is about an order of magnitude weaker[15], it is not negligible. Because of time-reversal symmetry, the spin splitting of bands at K and K' is opposite; the resulting band structure of monolayer 2H-MoS_2 relevant to realistic charge-carrier concentrations is schematically represented in Figure 5.

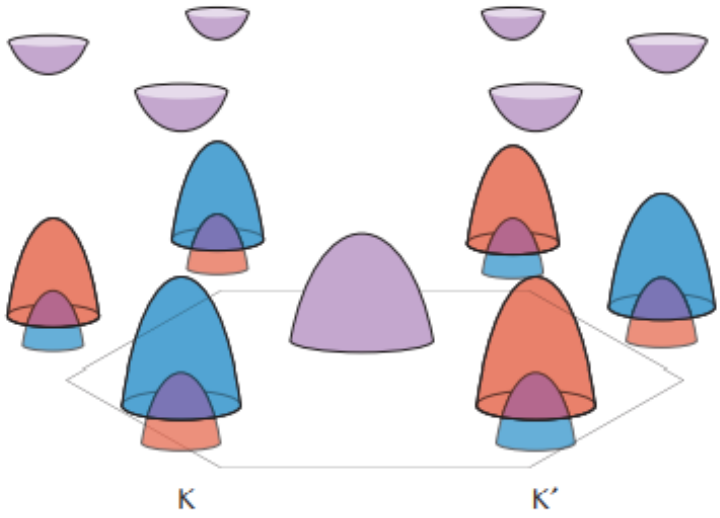

Figure 5: Schematic representation of the band structure of monolayer 2H-MoS_2, showing the spin splitting of the bands at the K and K' points on the corners of the Brillouin zone. Orange and blue colors indicate up and down spin polarization[10].

This property is referred to as spin–valley coupling[16] and implies that the valley polarization of charge carriers is automatically translated into their spin polarization. This intrinsic property of TMDs may be used to design spintronic devices that do not involve magnetic materials[17,18].

1.3 Excitons in TMDs

An exciton is a bound state between an excited electron in the conduction band, and an electron hole in the valence band of a semiconductor, bounded by the electrostatic Coulomb force. The formation of the exciton becomes possible when an incident photon with energy greater or equal that the bandgap of the material is absorbed. If the incident photon is absorbed, an electron is excited and moves from the valence band to the conduction band, leaving behind a hole in its position, which can be interpreted as quasiparticle with mass and spin equal to that of an electron but with positive charge (the absolute value of the hole charge is equal to that of an electron). The concept of an exciton is visualized in Figure 6.

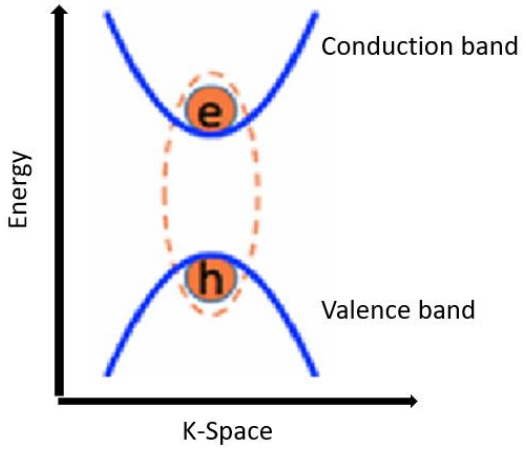

Figure 6: An electron-hole bound state[19]

An excitonic bound state that consists of a electron-hole pair is called neutral exciton often denoted as (X), and has an energy structure similar to that of a hydrogen atom. Also, charged excitons may be formed inside of a photoexcited 2D material. They are called trions (T) and can be positively or negatively charged. Thus, a pair of two electrons-one hole is a negatively charged trion (X^- or T^-) and a pair of two holes-one electron a positively charged trion (X^+ or T^+). In addition, given large exciton binding energies in 2D TMDs, any two of these aforementioned quasi-particles can sometimes combine to form either neutral (XX) or charged (XT) biexcitons[20]. These excitonic species are elementary quasi-particles in 2D materials and determine their many optoelectronic properties.

Figure 7: Representative formation of an exciton (X), trion (T), neutral biexciton (XX), and charged biexciton (XT) in TMDs

The exciton binding energy (E_b^X) is the energy difference between the material electronic bandgap (E_g) and its exciton PL peak energy (A^X), $E_b^X = E_g - A^X$. In other words, the exciton binding energy, is the amount of the energy needed to be given to the electron, in order to break the electron-hole pair from the binding state. Similarly, the biexciton binding energy (E_b^{XX}) is the energy difference between the exciton and biexciton (A^{XX}) peaks, $E_b^{XX} = A^X - A^{XX}$. Also, similarly to the biexciton, trions binding energy (E_b^T) is the difference between the exciton and trion (A^T) peaks ($E_b^T = A^X - A^T$). These binding energies can, therefore, be easily extracted from the PL spectra of the material. The definitions of these binding energies mentioned above are being illustrated schematically in Figure 8.

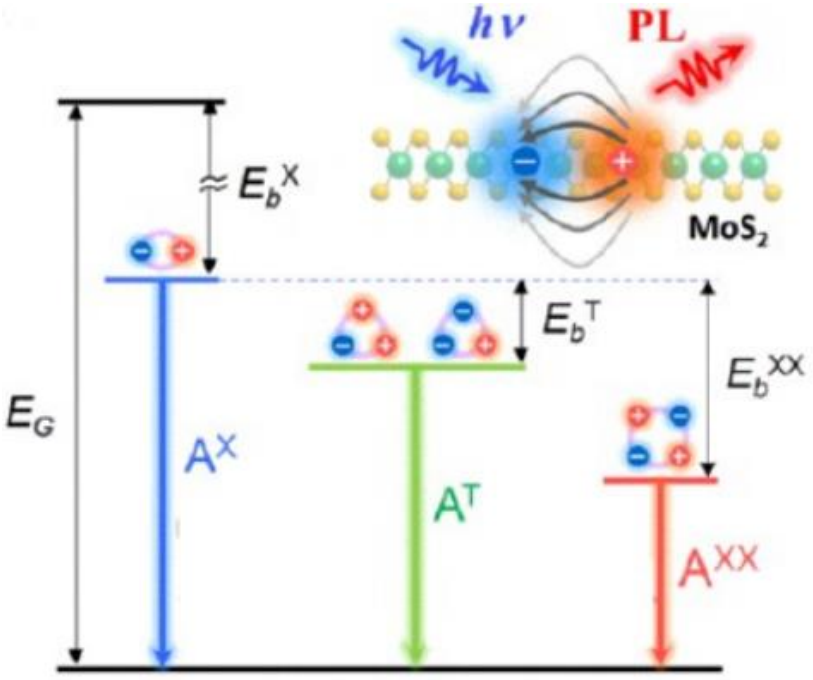

Figure 8: Binding energies of different many-body complexes. Illustrations of binding (E_b^X, E_b^T, and E_b^{XX}) and emission energies (A^X, A^T, and A^{XX}) for excitons, trions, and biexcitons, respectively[21].

Under excitation, the annihilation of the quasi-particles, including excitons, biexcitons, and trions, is accompanied by their distinct luminescence peaks. At room temperature, multilayered (ML) TMDs usually exhibit two distinctive exciton PL peaks associated with the spin−orbit coupling-induced splitting of the valence band edge, denoted as A and B, usually the A peak is more significant at room temperature conditions than the B peak[21].

1.4 Plasmons

When an incident light with fixed frequency hits a metal surface, it causes the free electrons on that surface to oscillate. The quantum of the charge density oscillation is called surface plasmon (SP). It has the same analogy of that of a phonon which is the quantization of mechanical vibrations. Plasmons, like excitons and phonons, are quasiparticles meaning they cannot be found outside of the metal and they exist only inside it. A Plasmon can be described in the classical picture as an oscillation of electron density with respect to the fixed positive ions in a metal[22].

There are two kinds of SPs, which called localized SPs (LSPs) and propagating SPs (PSPs or plasmonic waveguide). LSPs are oscillations of charge density that are confined on the surface of a metallic nanoparticle while PSPs are excitation of collective electrons that can only propagate near the vicinity of the interface. Both ideas are illustrated in Figure 9. [23]

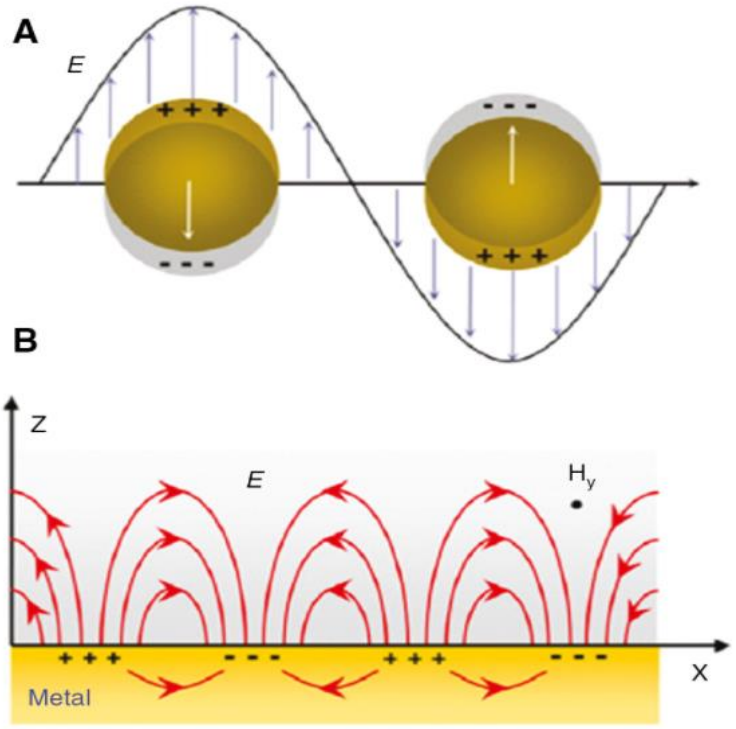

Figure 9: A visualization of a A) localized surface plasmon (LSP) oscillation under light excitation and B) propagating surface plasmon (PSP)[23].

1.5 Light Amplification of Stimulated Emission Radiation

Laser Amplification of Stimulated Emission Radiation (Laser), is an optical device that generates intense beam of coherent monochromatic light by stimulated emission of radiation. Laser light is different from an ordinary light. It has various unique properties such as coherence, monochromacity, directionality, and high intensity. Because of these unique properties, lasers are used in various applications especially in optoelectronics.

1.5.1 Principles of working of a laser

In lasers, photons are interacted in three ways with the atoms:

- Absorption of radiation
- Spontaneous emission
- Stimulated emission

1.5.1.1 Absorption of radiation

Absorption of radiation is the process by which electrons in the ground state absorbs energy from photons to jump into the higher energy level. In general, the electrons in the lower energy state can't jump into the higher energy state. They need sufficient energy in order jump into the higher energy state. When photons or light energy equal to the energy difference of the two energy levels ($E_2 - E_1$) is incident on the atom, the ground state electrons gains sufficient energy and jumps from ground state (E1) to the excited state (E_2)[24].

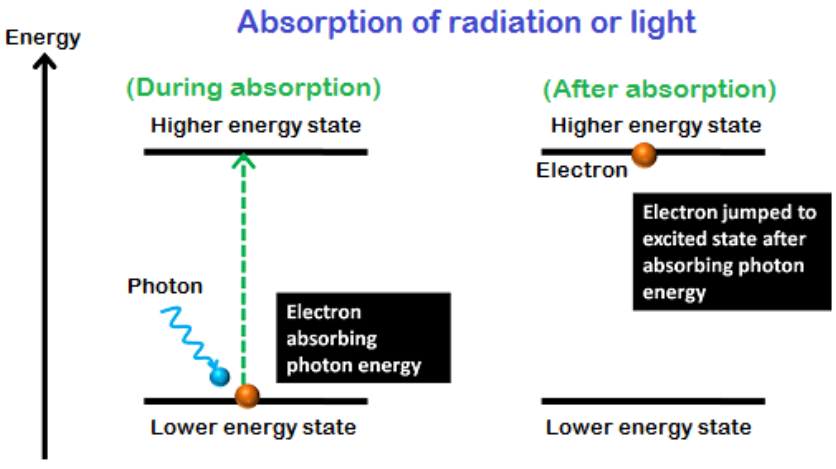

Figure 10: The mechanism of light absorption[24].

1.5.1.2 Spontaneous emission

Spontaneous emission is the process by which electrons in the excited state return to the ground state by emitting photons. The electrons in the excited state can stay only for a short period. The time up to which an excited electron can stay at higher energy state (E_2) is known as the lifetime of excited electrons. Typically, the lifetime of an excited state is approximately 10^{-8} seconds[24].

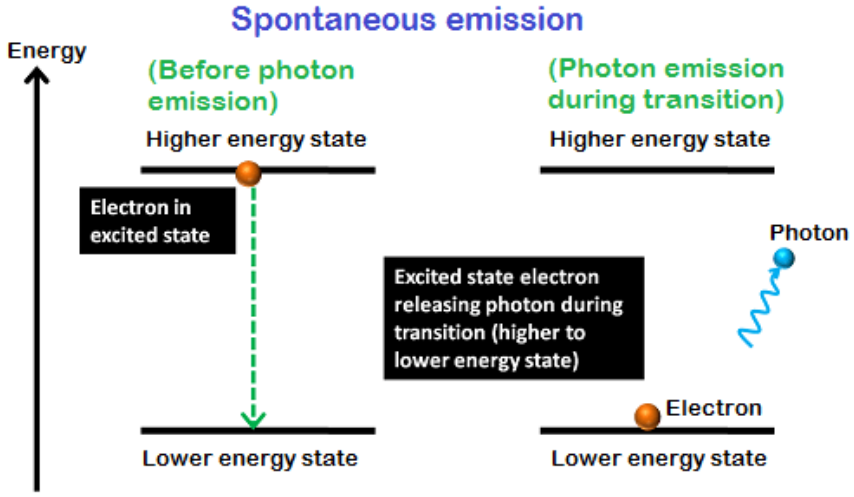

Figure 11: The mechanism of spontaneous emission[24].

1.5.1.3 Stimulated emission

Stimulated emission is the process by which incident photon interacts with the excited electron and forces it to return to the ground state. In stimulated emission, the light energy is supplied directly to the excited electron instead of supplying light energy to the ground state electrons. Unlike the spontaneous emission, the stimulated emission is not a natural process it is an artificial process, in addition, in stimulated emission the electrons in the excited state do not need to wait for completion of their lifetime. An alternative technique is used to forcefully return the excited electron to ground state before completion of their lifetime. This technique is known as the stimulated emission. This excited electron release energy in the form of light while falling to the ground state. When this mechanism takes place, two photons are emitted (one additional photon is emitted), one is due to the incident photon and another one is due to the energy release of excited electron.

Additionally, the stimulated emission process is very fast compared to the spontaneous emission process. All the emitted photons in stimulated emission have the same energy, same frequency and are in phase. Therefore, all photons in the stimulated emission travel in the same direction[24].

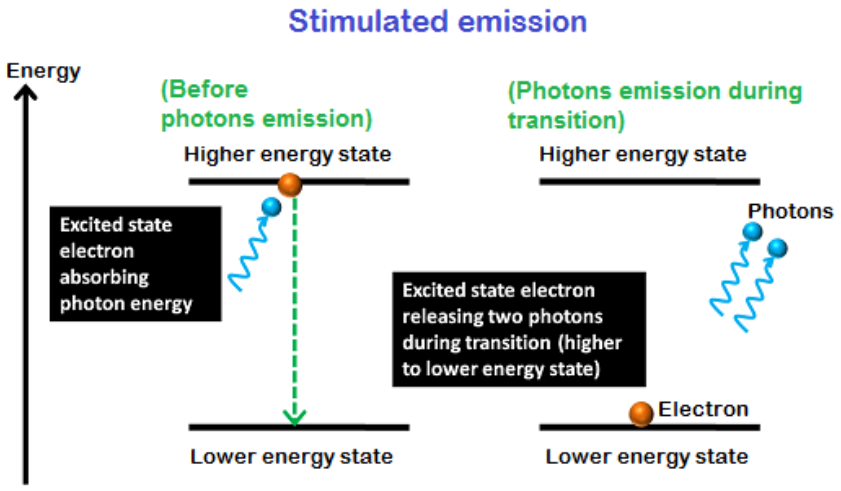

Figure 12: The mechanism of stimulated emission[24].

1.5.2 Population inversion

Population inversion is the process of achieving greater population of higher energy state as compared to the lower energy state. Population inversion technique is mainly used for light amplification. This mechanism is essential in order for the laser to operate. Population inversion however, cannot be achieved in a two-energy level system. Under normal conditions, the number of electrons (N_1) in the lower energy state (E_1) is always greater as compared to the number of electrons (N_2) in the higher energy state (E_2) (Figure 13). At best, an equal population of the two states can be achieved but this results in no optical gain.

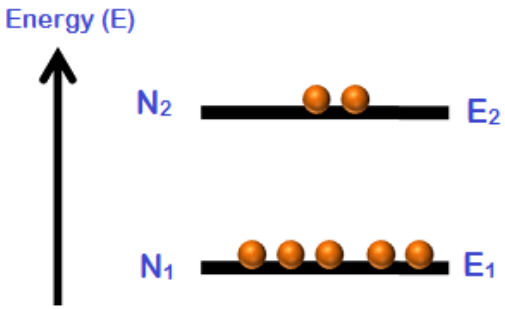

Figure 13: A two energy level system and the populations of each energy state[24].

Therefore, in order to achieve a successful population inversion, a three or more energy levels system is needed. The greater is the number of energy states the greater is the optical gain[24]. A simple three lever system is shown in Figure 14.

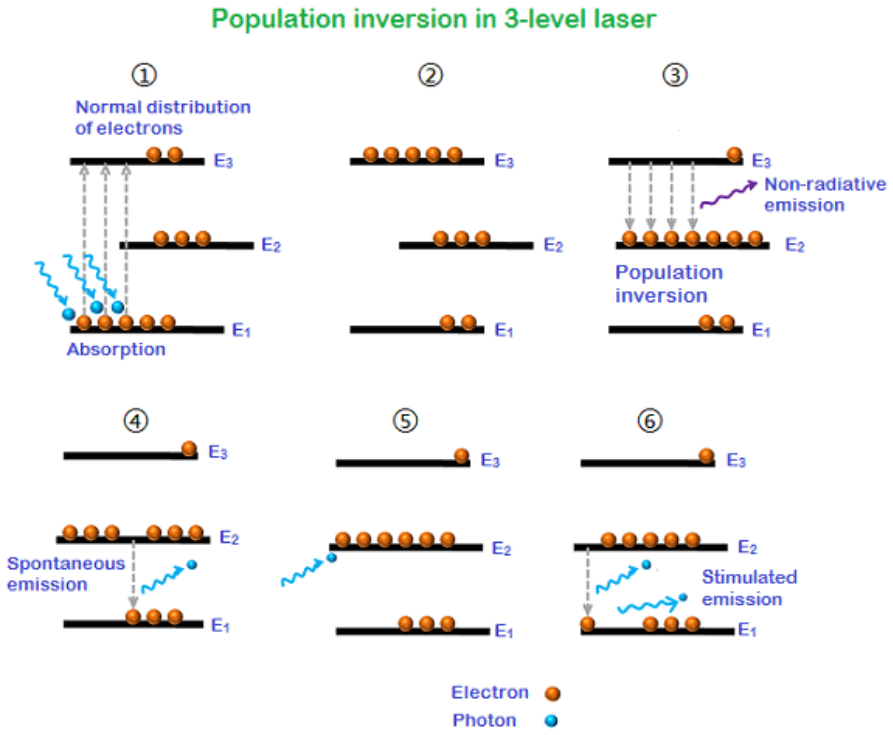

Figure 14: A typical illustration of a three-level population inversion system in six different phases[24].

To further understand this mechanism, lets assume the populations of the energy states E_1, E_2, E_3 with $E_1<E_2<E_3$ be N_1, N_2, N_3 with $N_1>N_2>N_3$. To get laser emission or population inversion, the population of higher energy state (E_2) should be greater than the population of the lower energy state (E_1). When we supply light energy which is equal to the energy difference of E_3 and E_1, the electrons in the lower energy state (E_1) gains sufficient energy and jumps into the higher energy state (E_3). This process of supplying energy is called pumping.

The lifetime of electrons in the energy state E_3 is very small as compared to the lifetime of electrons in the energy state E_2. Therefore, electrons in the energy level E_3 does not stay for long period. After that period, they quickly fall to the Meta stable state or energy state E_2 and releases non radiative energy instead of photons. The electrons in the Meta stable state E_2 will remain there for longer period because of its longer lifetime. As result, a large number of electrons accumulate in Meta stable state. Thus, the population of metal stable state will become greater than the population of energy states E_3 and E_1.

After completion of lifetime of electrons in the Meta stable state, they fall back to the lower energy state or ground state E1 by releasing energy in the form of photons through spontaneous emission. When this emitted photon interacts with the electron in the Meta stable state E_2, it forces that electron to fall back to the ground state. As a result, two photons are emitted through stimulated emission. This mechanism goes on and on and as a result millions of photon with the same energy and direction are emitted.

However, in a 3-level laser, at least half the population of electrons must be excited to the higher energy state to achieve population inversion. Therefore, the laser medium must be very strongly pumped. This makes 3-level lasers inefficient to produce photons or light. The three level lasers are the first type of lasers discovered. Nowadays Lasers are utilizing a four or higher energy level system[24]. An example of a 4-lever system is shown in Figure 15.

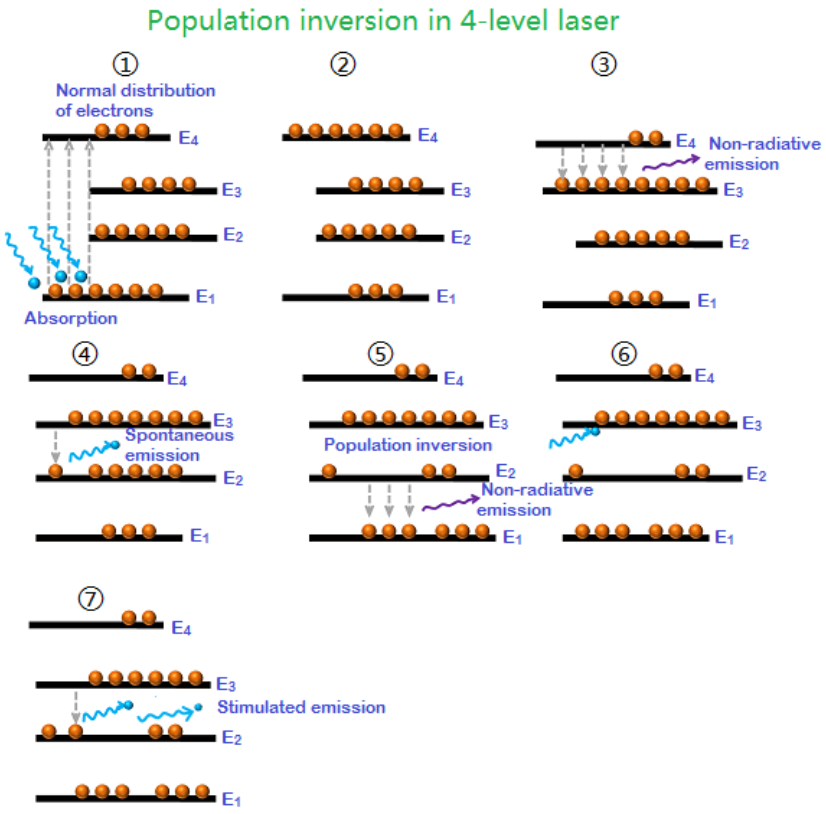

Figure 15: A four lever population inversion system[24].

In a 4-level laser, only a few electrons are excited to achieve population inversion. Therefore, a 4-level laser produces light efficiently than a 3-level laser.

1.5.3 Characteristics of a Laser

Laser light has four unique characteristics that differentiate it from ordinary light, there are:

- Coherence
- Directionality
- Monochromatic
- High intensity

1.5.3.1 Coherence

The photons emitted from ordinary light sources have different energies, frequencies, wavelengths, or colors. Hence, the light waves of ordinary light sources have many wavelengths. Therefore, photons emitted by an ordinary light source are out of phase.

In laser however, the electron transition occurs artificially. In other words, in laser, electron transition occurs in specific time. All the photons emitted in laser have the same energy, frequency, or wavelength. Hence, the light waves of laser light have single wavelength or color. Therefore, the wavelengths of the laser light are in phase in space and time. Light generated by laser is highly coherent, so because of this coherence, a large amount of power can be concentrated in a narrow space[24].

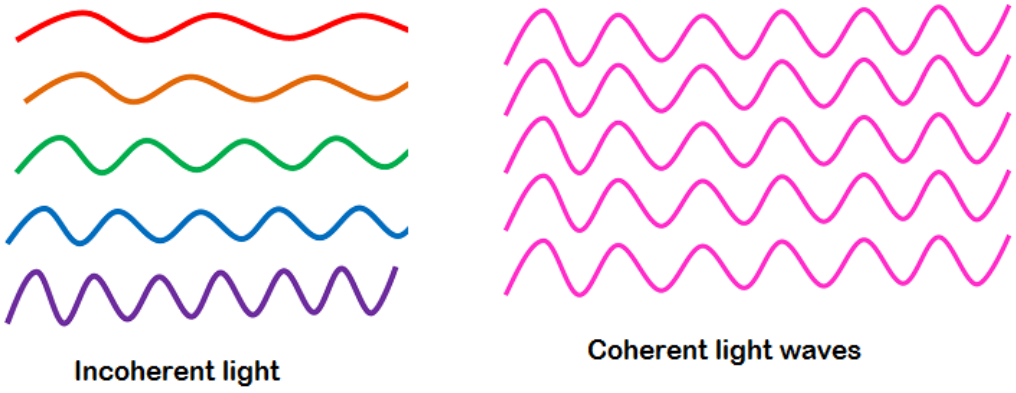

Figure 16: Incoherent (left) and Coherent (right) radiation[24]

1.5.3.2 Directionality

In conventional light sources (lamp, sodium lamp and torchlight), photons will travel in random direction. Therefore, these light sources emit light in all directions. On the other hand, in laser, all photons will travel in same direction. Therefore, laser emits light only in one direction. This is called directionality of laser light. The width of a laser beam is extremely narrow. Hence, a laser beam can travel to long distances without spreading[24].

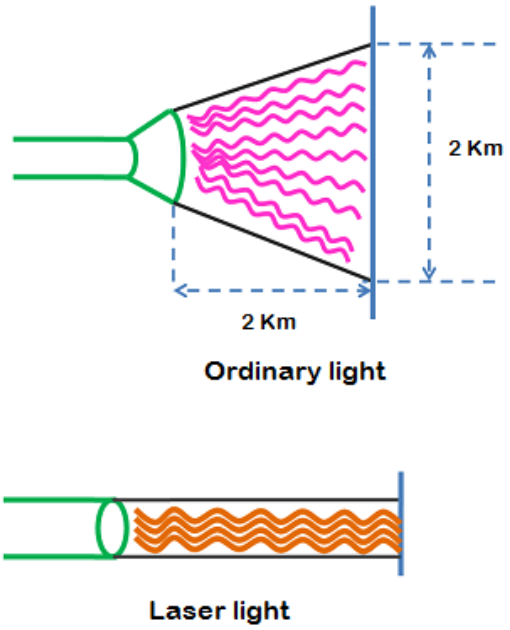

Figure 17: The directionality of a conventional light source (top) and a laser source (bottom)[24]

1.5.3.3 Monochromatic

Monochromatic light means a light containing a single color or wavelength. The photons emitted from ordinary light sources have different energies, frequencies, wavelengths, or colors. Hence, the light waves of ordinary light sources have many wavelengths or colors. Therefore, ordinary light is a mixture of waves having different frequencies or wavelengths. On the other hand, in laser, all the emitted photons have the same energy, frequency, or wavelength. Hence, the light waves of laser have single wavelength or color. Therefore, laser light covers a very narrow range of frequencies or wavelengths[24].

1.5.3.4 High intensity

The intensity of a wave is defined as the energy per unit time flowing through a unit normal area. In an ordinary light source, the light spreads out uniformly in all directions. In laser, the light spreads in a small region of space and in a small wavelength range. Hence, laser light has greater intensity when compared to the ordinary light[24].

1.5.4 Laser construction

A laser system consists of three important components:

- Pump source
- Medium
- Optical resonator

1.5.4.1 Pump source

The pump source or energy source is the part of a laser system that provides energy to the laser medium. The source of energy supplies sufficient amount of energy to the laser medium by which the electrons in the lower energy state are excited to the higher energy state. As a result, we get population inversion in the active medium or laser medium. Examples of energy sources include electric discharges, light from another laser, chemical reactions, and flash lamps. The type of energy source used is mostly depends on the laser medium. For example, Excimer laser uses chemical reaction as energy source, a Helium laser uses an electric discharge as energy source and Nd:YAG laser uses light focused from diode laser as energy source[24].

1.5.4.2 Medium

The laser medium is a medium where spontaneous and stimulated emission of radiation takes place. If we use electrical energy as energy source then a single photon or few photons (which are produced spontaneously) will produce large number of photons by stimulated emission process. Thus, light amplification is achieved in laser medium. Laser medium is also known as active medium or gain medium. The laser medium will determine the characteristics of the laser light emitted. The laser medium can be solid, liquid, or gaseous[24].

1.5.4.3 Optical resonator

The laser medium is surrounded by two parallel mirrors which provides feedback of the light. One mirror is fully reflective (100 % reflective) whereas another one is partially reflective (<100 % reflective). These two mirrors as a whole is called optical resonator. Optical resonator is also known as optical cavity or resonating cavity. These two mirrors are given optical coatings which determine their reflective properties. Optical coating is a thin layer of material deposited on materials such as mirror or lens. Each mirror is coated differently, therefore, each mirror will reflect the light differently. One mirror will completely reflect the light whereas another one will partially reflect the light. The completely reflective mirror is called high reflector whereas the partially reflective mirror is called output coupler. The output coupler will allows some of the light to leave the optical cavity to produce the laser's output beam[24].

The light generated within the laser medium will bounce back and forth between the two mirrors. This stimulates other electrons to release light while falling to the ground state. Likewise, a large number of electrons are stimulated to emit light. Thus, optical gain is achieved. Then, the amplified light escapes through the partially reflecting mirror. The light in the laser medium is reflected many hundreds of times between the mirrors before it escapes through the partially reflecting mirror. Hence, this light will travel to large distances without spreading in the space[24].

A Laser system is schematically illustrated in figure 18.

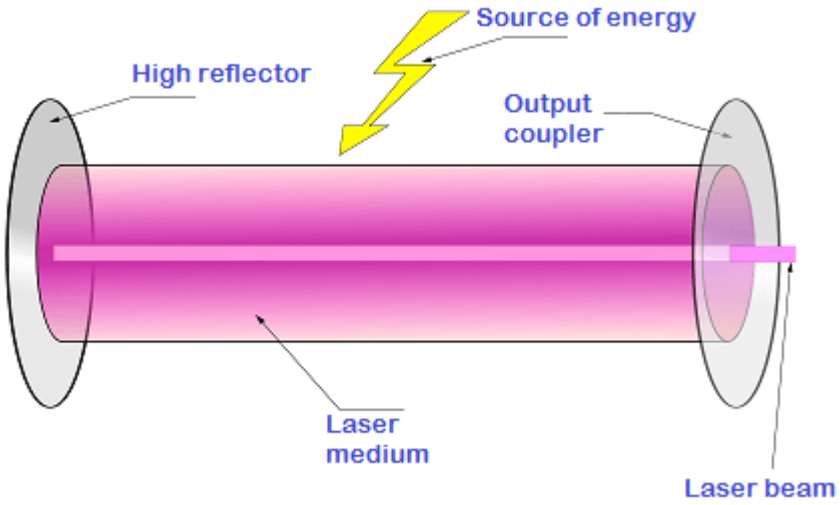

Figure 18: A typical laser system[24].

1.6 Laser-induced periodic surface structures (LIPSS)

Laser-induced periodic surface structures (LIPSSs) are regular wavy surface structures with dimensions usually in the sub-micrometer range, which can develop on the surface of many materials exposed to laser radiation. The most common type of LIPSSs, which can be produced with continuous wave lasers or pulsed lasers, have a periodicity close to the laser wavelength and a direction orthogonal to the polarization of the laser radiation. They are usually referred to as low spatial frequency LIPSSs (LSFLs). It is generally accepted that these LIPSSs are the result of the interaction of the laser radiation with the rough surface of the material. The "Sipe theory"[25] is commonly considered to be the most adequate theoretical description of this interaction[26].

The Sipe theory provides an analytical solution of Maxwell's equations regarding the interaction of electromagnetic waves with rough surfaces. The main outcome of this theory is the prediction of the frequency domain spectrum of the absorbed laser energy just below the rough surface of the material. The spectrum shows that the interaction of electromagnetic waves with rough surfaces results in a periodic energy profile, with a periodicity close to the wavelength of the laser radiation, in the direction orthogonal to the polarization. The type of LIPSSs obtained depends on the optical properties of the material and on the quantity of material removed per iteration. LIPSSs are found to be the fingerprints of the interaction of electromagnetic waves with rough surfaces. Each kind of LIPSSs has a specific signature in the frequency domain. When applying picosecond or femtosecond laser pulses, ripples with a periodicity significantly smaller than the laser wavelength and an orientation either parallel or orthogonal to the polarization, referred to as high spatial frequency LIPSSs (HSFLs), can develop. The HSFLs renewed the interest of researchers in the topic because, from a practical point of view, HSFLs show a strong potential for surface nanostructuring due to their small dimensions[26].

1.6.1 The sipe theory

The Sipe theory was published in 1983 by Sipe and his coworkers [25]. The goal of this theory is to explain LIPSS formation, and particularly LSFL formation since almost no HSFLs were observed before the 2000s. In the frame of this approach, LIPSSs are thought to be the fingerprints of the inhomogeneous absorption of the laser light below the rough surface of materials. To prove this assertion, Sipe et al. proposed a careful treatment of the interaction of electromagnetic waves with rough surfaces. The concept of the Sipe theory is shown in Figure 19. The incident laser radiation interacts with the rough surface, leading to an inhomogeneous energy absorption. The main outcome of the Sipe theory is the prediction of the distribution of the absorbed energy just below the rough surface of the material (dotted line). This prediction is made by solving Maxwell's equations analytically for a plane wave incident on the rough surface. These equations, as well as the resulting absorbed energy are calculated in the frequency domain. The spatial frequency spectrum, referred to as Sipe theory calculations in Figure 19,

shows white sharp peaks indicating that the absorbed energy is periodic. Since LIPSSs are assumed to grow where the absorbed energy is the largest (represented by the radiating dots) in the Sipe theory, their formation follows the absorbed energy profile. Therefore, a Fourier transform of the height profile of a surface with LIPSSs is directly comparable to the absorbed energy below the rough surface. These Fourier transforms can be obtained by studying diffraction patterns produced by a coherent light source, e.g. a continuous wave laser, reflected from a surface with LSFLs [26].

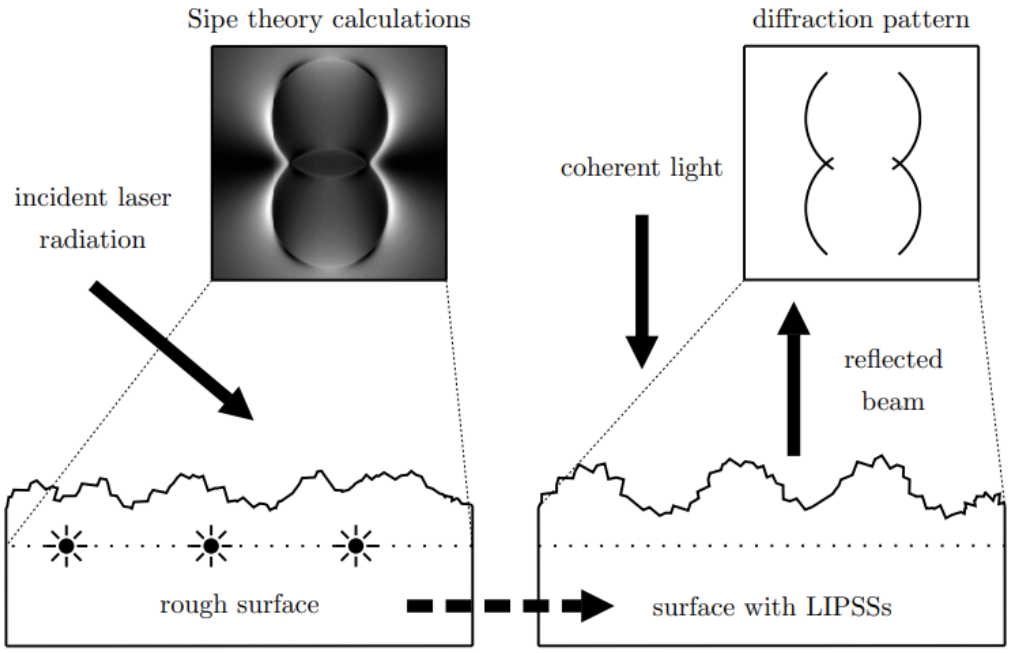

Figure 19: Concept of the Sipe theory. The radiating dots just below the rough surface symbolize the locations where the absorbed energy is the largest. The dashed arrow represents the assumption that LIPSS formation occur where the absorbed energy is the largest. The thin dashed lines indicate a frequency domain representation of the absorbed energy (Sipe theory calculations) and the height profile of the rough surface with LIPSSs (diffraction pattern)[26].

1.6.2 Characteristics of laser-induced periodic surface structures

The spatial characteristics, i.e. periodicity, height and orientation, of LIPSSs depend on material properties and on the laser parameters, such as the wavelength and the polarization of the laser radiation. However, many other parameters are involved in LIPSS formation. However, many other parameters are involved in LIPSS formation. The laser beam is described by its wavelength λ, angle of incidence θ and direction of polarization[26]. In most cases, the applied polarization is linear but LIPSS formation has also been investigated for circular [27,28], elliptical [29,30] or even radial and azimuthal polarized light [31]. The energy of the pulse E_p is usually described by the fluence ϕ (energy per surface area) applied to the surface of the material. The number of subsequent pulses

N applied to the same location on the surface also affects LIPSSs characteristics. Figure 20 shows the main parameters influencing LIPSSs principal characteristics, which are their periodicity Λ, height (peak to valley) h and orientation[26].

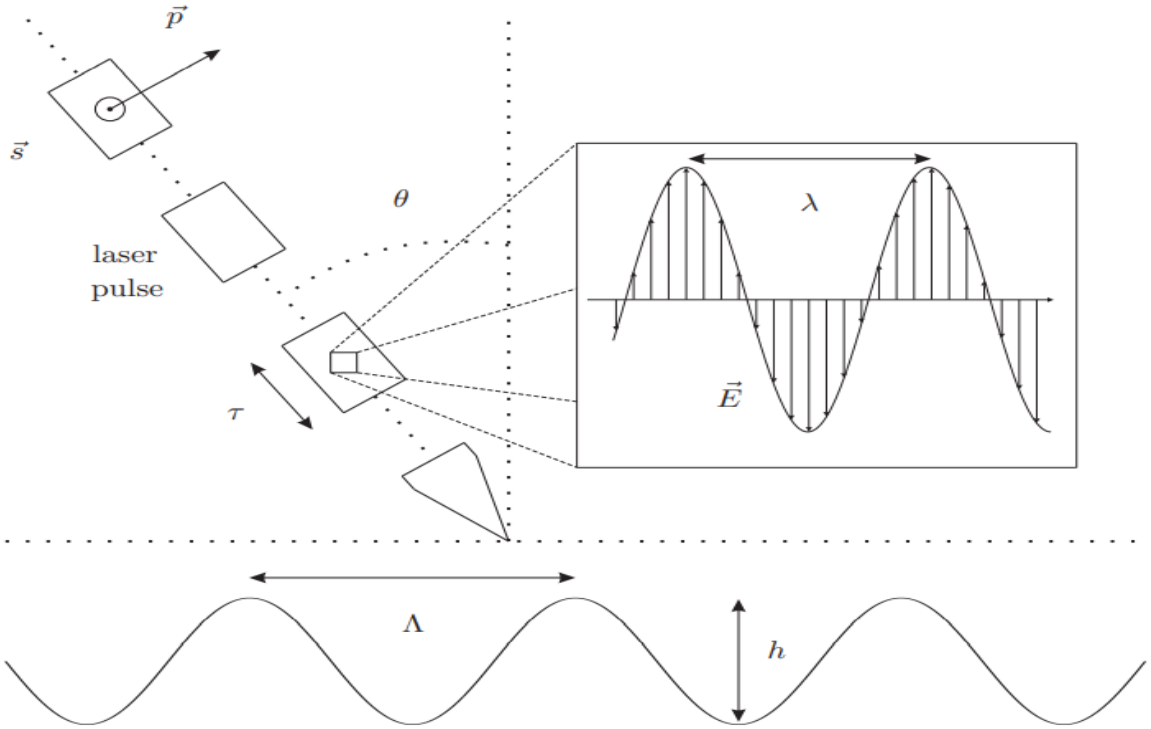

Figure 20 : The main parameters and the notations used to describe LIPSSs as well as the laser parameters. λ is the wavelength of the laser light, θ the angle of incidence, τ the pulse duration, $\vec{p}$ the component of the laser beam polarization parallel to the plane of incidence, $\vec{s}$ the component of the laser beam polarization orthogonal to the plane of incidence, $\vec{E}$ the electric field, Λ the periodicity of LIPSSs and h the height (peak to valley) of LIPSSs[26].

1.6.3 Low spatial frequency laser-induced periodic surface structures

Low spatial frequency LIPSSs (LSFLs) are the most observed kind of LIPSSs. They have been observed on metals[32], semiconductors[29,31] and dielectrics[32]. At normal incidence of the laser beam, LSFLs show a periodicity close to the laser wavelength (Λ ≈ λ), a height in the range of a few hundreds of nanometers[33,34] and a direction orthogonal to the polarization of the laser radiation. LSFLs can be obtained with continuous wave lasers[35] as well as pulsed lasers[36,37] when several pulses are applied to the same location of the surface of the material. The number of pulses required to create LSFLs is low (less than 100)[38–40], but a higher number of pulses can also lead to their formation[41]. If the subsequent laser pulses are partially overlapping, instead of applied to the same location on the surface, LSFLs can also occur and

extend over several laser spots[42,43]. The fluence regime, in which LSFLs grow, is close to the fluence threshold at which the material starts to ablate for a single pulse, referred to as single pulse ablation threshold[44,45]. It is worth noting that the fluence applied also affects the height of LSFLs[46].

From the above-mentioned description, the properties of LSFLs can vary significantly. For example, the angle of incidence of the laser beam has a strong influence on the periodicity and orientation of LSFLs[47,48]. At normal incidence of the laser beam, LSFLs can also show different characteristics. In several cases, the periodicity of LSFLs does not follow strictly the laser wavelength. This characteristic has been observed mainly for ultra-short laser pulses and concerns all types of materials. It is worth noting that the periodicity of LSFLs decreases with increasing number of pulses applied and that the rate of this decrease is also material dependent[49].

1.6.4 High spatial frequency laser-induced periodic surface structures

High spatial frequency LIPSSs (HSFLs) can be produced on metals[50,51], semiconductors[52,53] and dielectrics [54,55]. They are defined as LIPSSs with a periodicity Λ significantly smaller than the laser wavelength λ ($\Lambda \ll \lambda$). On the contrary to LSFLs, HSFLs develop almost only for pulsed lasers, when the pulses applied are in the picosecond of femtosecond regime. For linearly polarized light, HSFLs are oriented parallel[56,57] or orthogonal [58,59] to the polarization of the laser light. Both orientations, orthogonal or parallel to the laser polarization, have been observed for the different types of materials. The fluence regime in which HSFLs grow is below or close to the single pulse ablation threshold [58,60]. Depending on the material and on the processing conditions, the periodicity of HSFLs increases with the laser wavelength [59] or remains constant [60]. The same holds for the angle of incidence, i.e. HSFLs can be sensitive [58] or insensitive [60] to a variation of the angle of incidence.

1.6.5 Conclusions on LIPSS

Laser-induced periodic surface structures (LIPSSs) created with linearly polarized femtosecond laser radiation, under normal incidence of the laser beam, can be classified mainly into LSFLs and HSFLs. These two types of LIPSSs have two properties in common: their periodicities depend on the wavelength of the laser radiation and their directions depend on the polarization of the laser light. This strongly suggests that LIPSS formation can be understood in the framework of an electromagnetic theory[26].

Chapter 2: Characterization techniques principles

2.1 Raman spectroscopy

The Raman effect was discovered in 1928 by the Indian physicist C.V. Raman[61]. This method describes the inelastic scattering of photons on a quantized molecular system. In most cases, the vibrational states of molecules are utilized as scattering system and that is why Raman spectroscopy is often referred to as a vibrational spectroscopic technique. Vibrational Raman spectroscopy is a complementary method to IR absorption spectroscopy. The two approaches differ in their physical origin: while IR absorption describes the direct absorption of an IR photon to excite a vibrational quantum (i.e. one photon absorption process), in Raman spectroscopy as mentioned above the vibrational excitation takes place via a two-photon scattering process. In IR absorption spectroscopy vibrational modes leading to a change in the dipole moment during the vibration can be excited, while for Raman active vibrations the polarizability has to change. Since molecular vibrations are distinct for every molecule, vibrational spectra can therefore be interpreted as a type of characteristic “molecular fingerprint” of an examined inorganic, organic or biological molecule or more complex systems like e.g. biological cells and tissue[62]. Thus, vibrational spectroscopy is applied for the qualitative and quantitative analysis in chemistry, biology, material and life sciences and biomedicine. However, while the molecular selectivity of Raman spectroscopy is very high its sensitivity is very low, i.e. the Raman scattering process is characterized by small Raman cross-sections. In general, only one photon out of 10^8 photons is scattered inelastically. Several Raman signal-enhancing techniques increasing the intrinsically weak Raman scattering cross-sections by several orders of magnitude are known. The two most prominent approaches are Resonance Raman spectroscopy (RRS) and Surface Enhanced Raman Spectroscopy (SERS)[63].

2.1.1 Principles of Raman spectroscopy

In the IR spectrum range, three types of scattering types can take place: Rayleigh scattering, Stokes scattering and Anti-Stokes scattering. Raman shifted photons can be of either higher or lower energy, depending upon the vibrational state of the molecule under study.

The Rayleigh scattering is elastic which means that the total energy between the incident and the scattered photon is conserved. On the other hand, the Stokes and Anti-Stokes scattering are inelastic, meaning that the total energy between the incident and the scattered photon in not conserved. Stokes radiation occurs at lower energy (longer wavelength) than the Rayleigh radiation, and anti-Stokes radiation has greater energy. The energy increase or decrease is related to the vibrational energy levels in the ground electronic state of the molecule, and as such, the observed Raman shift of the Stokes and anti-Stokes features are a direct measure of the vibrational energies of the molecule. There three mechanisms are illustrated in figure 21.

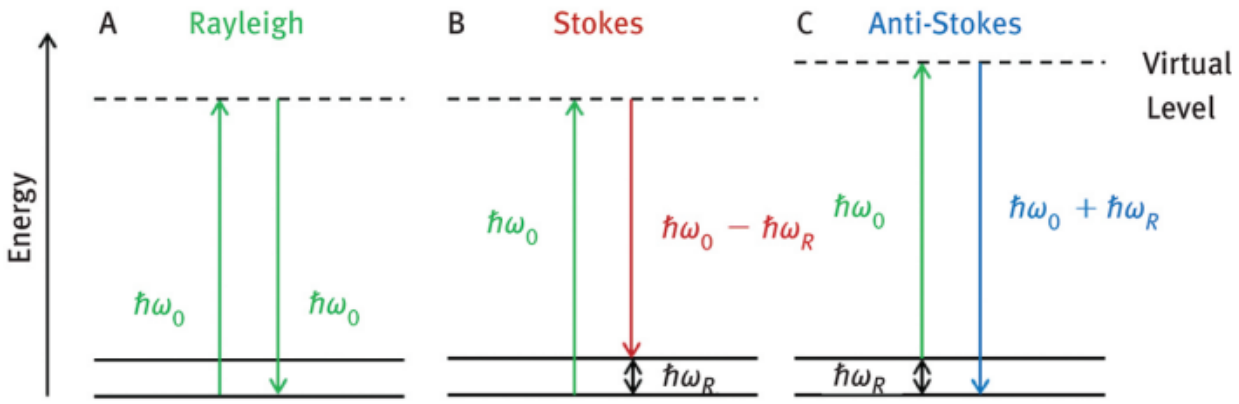

Figure 21: Schematical illustration of A) The Rayleigh scattering process where the initial and final scattering states are identical, B) Stokes scattering in witch energy is transferred from the photon to the molecule, i.e. the final scattering state is an excited quantum state. C) Anti-Stokes scattering which is the case when the molecule originally resides in an excited quantum state and the scattering process can end in the ground state, here energy is transferred from the molecular quantum system to the photon[63].

In the case of vibrational Raman spectroscopy, the depicted quantum states in Figure 21 are vibrational levels. According to the Boltzmann distribution, the vibrational ground state is significantly more populated than the energetically excited vibrational states at room temperature. Consequently, the intensity of the Stokes Raman scattering is larger than the intensity of the anti-Stokes Raman scattering. To conclude, the inelastic Raman scattering can be associated with a change in vibrational, rotational or electronic energy, i.e. Raman scattering is performed on quantized systems and the energy is exchanged between the molecules and the incident photons. The exchanged energy is related to the energy levels of vibrational, rotational or electronic transitions. However, as mentioned above the majority of the reported Raman spectroscopic studies are based on the vibrational Raman effect, and thus Raman spectroscopy is often defined as vibrational spectroscopy, being complementary to IR spectroscopy[63].

When plotting Raman spectra, relative wavenumber values are displayed, i.e. the shift of the inelastic scattered light in relation to the applied excitation wavelength (in contrast, IR spectra are plotted in absolute wavenumber values). As already mentioned, the Stokes Raman vibrational modes have a higher intensity than the anti-Stokes Raman lines, and thus the Stokes Raman spectrum is usually recorded[63]. A typical Raman spectrum of MoS_2 is presented in figure 22.

However, Raman spectroscopy is known as a spectroscopic method with a very high amount of molecular information, as mentioned above, its sensitivity is rather poor. Roughly one photon out of 10^8 photons is scattered inelastically, and thus the integration times can become very long as well as the observation of molecules and substances in low concentrations is limited. The two most prominent approaches with the aim to improve the sensitivity of the technique are Resonance Raman spectroscopy (RRS) and Surface Enhanced Raman Spectroscopy (SERS).

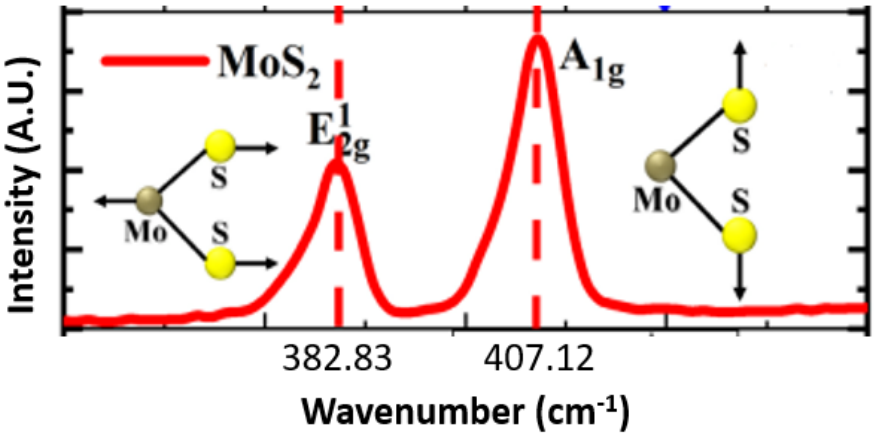

Figure 22: Raman spectra of MoS_2 featuring its E_{2g} (in plane) and A_{1g} (out of plane) vibrational modes[9].

2.1.2 Typical Raman spectrometer components

There are three primary components to any Raman spectrometer: an excitation source, a sampling apparatus, and a detector. While these three components have come in varying forms over the years, modern Raman instrumentation has developed around using a laser as the excitation source, a spectrometer for the detector, and either a microscope or a fiber optic probe for the sampling apparatus[64].

2.1.2.1 Excitation source (LASER)

Since Raman spectroscopy is predicated on the ability to measure a shift in wavelength (or frequency) it is imperative that a monochromatic excitation source should be employed. While a laser is typically the best excitation source, not all lasers are suitable for Raman spectroscopy, so it is essential that the laser frequency is extremely stable and does not mode hop, since this will cause errors in the Raman shift. It is also essential to utilize a clean, narrow bandwidth laser because the quality of the Raman peaks is directly affected by the sharpness and stability of the excitation light source. The final consideration when deciding which laser to use for a Raman spectrometer is the wavelength. The shorter the wavelength, the more powerful the Raman signal. Most organic molecules will tend to fluoresce when excited by high energy (short wavelength) photons. Although fluorescence is typically considered to be a low light level process, it can still overwhelm the signal in the Raman spectrum. his is because the Raman effect is comprised of a very small fraction (about 1 in 10^8) of the incident photons. As a result, visible lasers are typically only used for inorganic materials such as carbon nanotubes[64]. For increased sensitivity with inorganic molecules (such as MoS_2), a 532nm laser is the best choice because fluorescence is no longer an issue.

2.1.2.2 Detector (Spectrometer)

As previously discussed, Raman scattering is very weak and therefore tends to require long integration times in order to collect enough photons to measure a discernible signal. This makes the use of a thermoelectrically-cooled spectrometer a requirement in order to reduce the dark noise. For very low concentrations or weak Raman scatters, it may be necessary to use a back-thinned CCD to further increase the sensitivity of the spectrometer. By etching the detector to only a few microns thick, the probability of an electron being reabsorbed as it travels through the detector based on Beer's law[65] is greatly reduced. This increases the sensitivity of the detector from a maximum quantum efficiency of 35% to greater than 90% [64].

Due to the highly selective nature of Raman spectra, they may contain peaks which are fairly close together. Depending on the application, it may be necessary to resolve these closely spaced peaks, which requires the use of a high resolution spectrometer. Typically, standard spectrometer configurations are for 532nm and 785nm laser excitation wavelengths, with custom excitation wavelengths also available. These spectrometers can offer a variety of configurations specially designed for wide spectral range and high resolution. Typical spectral ranges are available from as low as 65cm^{-1} (filter dependent) to as high as 4000cm^{-1}, with a spectral resolution as fine as 3cm^{-1} [64].

2.1.2.3 Sampling apparatus

When measuring the sample, there is no more effective method of directing the laser light to the sample, collecting the Raman scatter, and directing it to a spectrometer than a fiber optic probe. A Raman probe must be capable of directing and focusing the monochromatic excitation source (typically a laser) to the sample, collecting the scattered light and then directing it to the spectrometer. A typical Raman probe is shown in Figure 23.

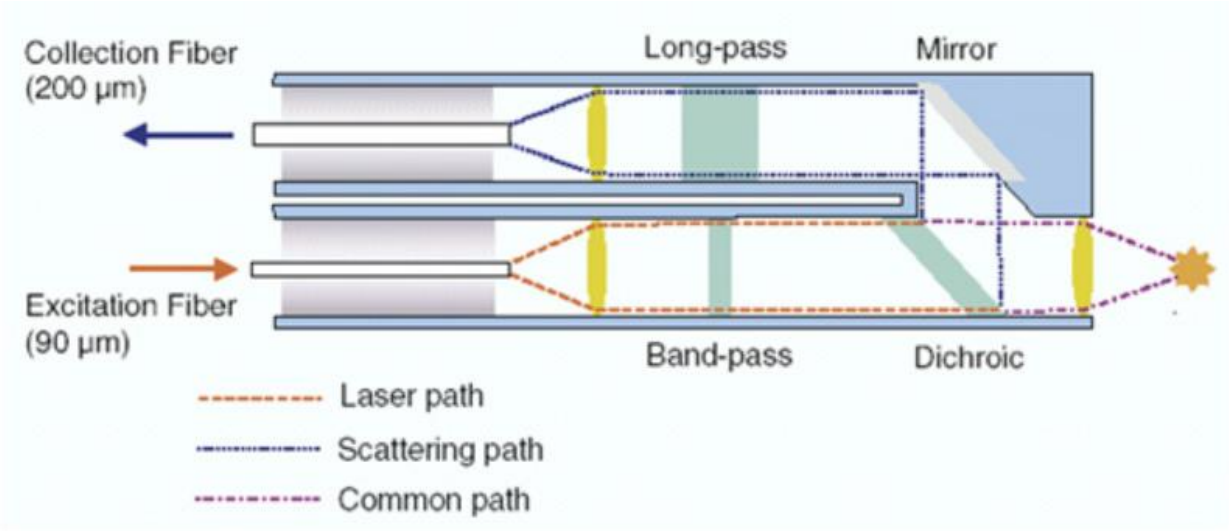

Figure 23: A Raman probe configuration[64].

Since a pure signal is extremely important to Raman spectroscopy, a narrow band-pass filter is placed in the optical path of the excitation source before it reaches the sample. It is also important to note that since the Raman effect is extremely weak, the signal must be collected at a 0^{o} angle normal to the sample. This causes interference from Rayleigh scattering and therefore it is essential to filter the collected signal through the use of a long pass filter before it is directed to the spectrometer.

The flexibility afforded by fiber optics not only allows for the probe to be taken to a solid sample, but also allows it to be immersed in liquids or slurries in both laboratory and process environments (for real time kinetic measurements). It can also be connected to microscopes, cuvette holders, as well as a plethora of sampling accessories[64].

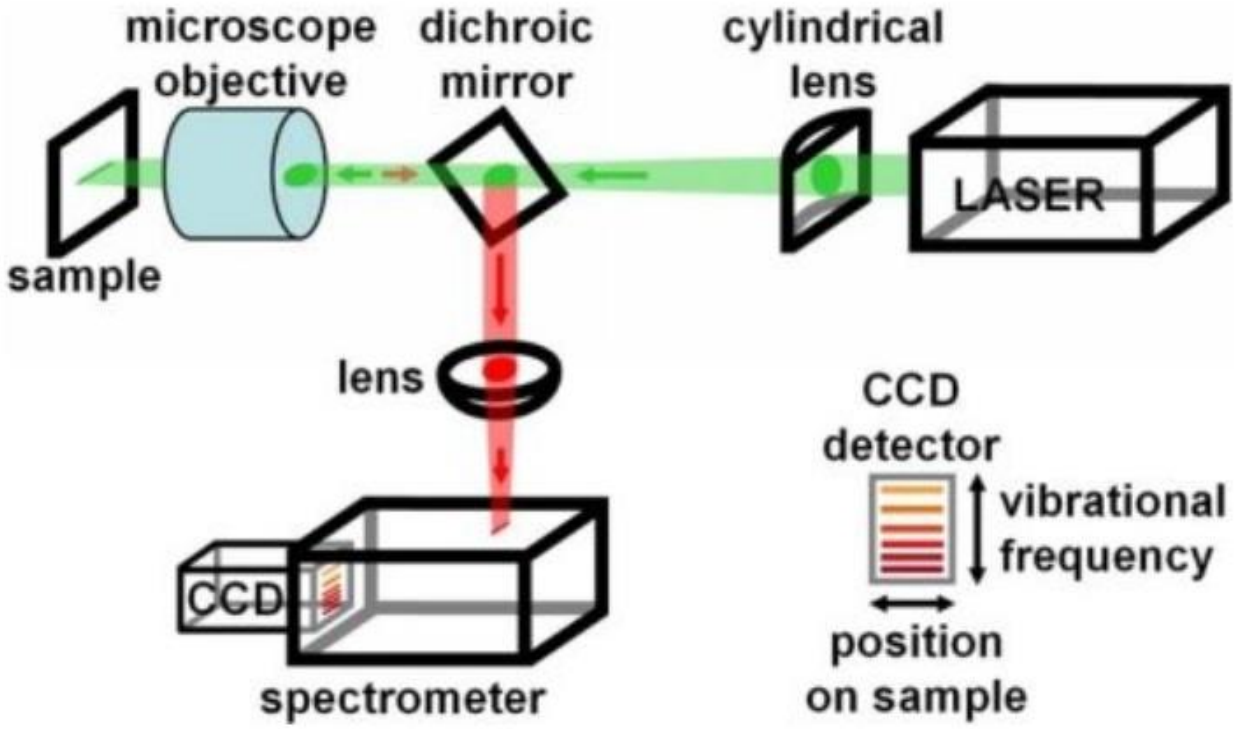

Figure 24: Schematic of Raman spectrometer. The displayed set-up focuses the illuminating laser (colored green) down to a line on the sample (slit scanning mode), which can be replaced by a spot by removing the cylindrical lens. When a spot is illuminated at the sample, the Raman-shifted light (colored red) is filtered out from the laser light by a dichroic mirror, and dispersed along a vertical line on the two dimensional CCD detector. In slit-scanning mode, many spectra are acquired simultaneously: each position along the line on the sample produces a spectrum along the CCD detector[66].

2.2 Photoluminescence spectroscopy

Photoluminescence spectroscopy is a contactless, nondestructive method of probing the electronic structure of materials. Light is directed onto a sample, where it is absorbed and imparts excess energy into the material in a process called photo-excitation. One way this excess energy can be dissipated by the sample is through the emission of light, or luminescence. In the case of photo-excitation, this luminescence is called photoluminescence[67].

2.2.1 Principles of Photoluminescence spectroscopy

Photo-excitation causes electrons within a material to move into permissible excited states. When these electrons return to their equilibrium states, the excess energy is released and may include the emission of light (a radiative process) or may not (a nonradiative process). The energy of the emitted light (photoluminescence) relates to the difference in energy levels between the two electron states involved in the transition between the excited state and the equilibrium state. The quantity of the emitted light is related to the relative contribution of the radiative process[67]. An example of this mechanism is a semiconductor shown in Figure 25.

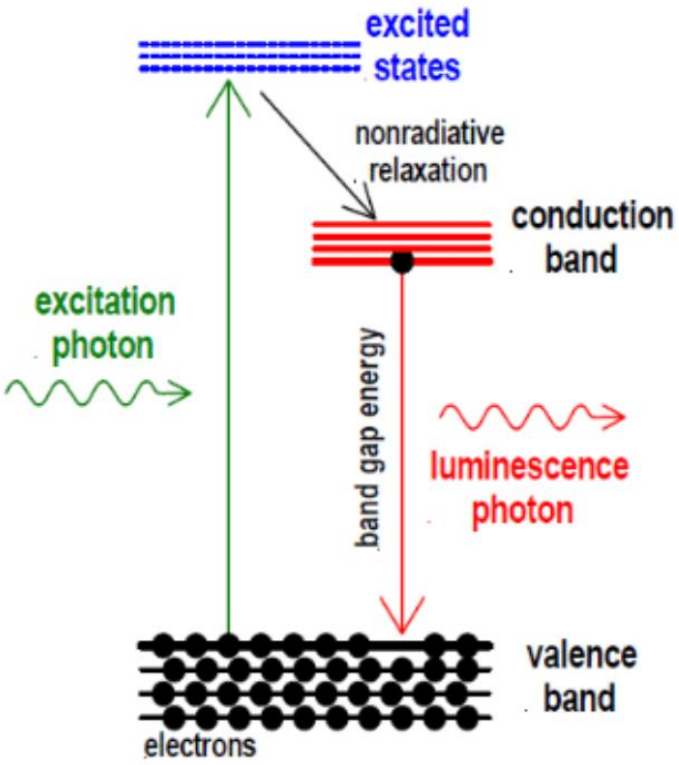

Figure 25: Photoluminescence mechanism in a semiconductor energy structure[68].

In most photoluminescent systems chromophore aggregation generally quenches light emission via aggregation-caused quenching (ACQ). This means that it is necessary to use and study fluorophores in dilute solutions or as isolated molecules. This in turn results in poor sensitivity of devices employing fluorescence, e.g., biosensors and bioassays. However, there have recently been examples reported in which luminogenic aggregation played a constructive, instead of destructive role in the light-emitting process. This aggregated-induced emission (AIE) is of great potential significance in particular with regard to solid state devices. Photoluminescence spectroscopy provides a good method for the study of luminescent properties of a fluorophore[67].

However, compared with other optical methods of characterization like reflection and absorption, PL is less stringent about beam alignment, surface flatness, and sample thickness. Another shortcoming of PL is the difficulty in estimating the density of interface and impurity states. When these states have radiative levels, they are readily identified in the PL spectrum, and the size of the associated PL peaks provides a relative measure of their presence in the sample. However, measuring the absolute density of these states is a far more formidable task and typically requires an exhaustive analysis of the excitation intensity dependence of the PL signal

2.2.2 Forms of photoluminescence

There are three major forms of photoluminescence:

- Resonant radiation
- Fluorescence
- Phosphorescence

2.2.2.1 Resonant radiation

In resonant radiation, a photon of a particular wavelength is absorbed and an equivalent photon is immediately emitted, through which no significant internal energy transitions of the chemical substrate between absorption and emission are involved and the process is usually of an order of 10 nanoseconds[67].

2.2.2.2 Fluorescence

When the chemical substrate undergoes internal energy transitions before relaxing to its ground state by emitting photons, some of the absorbed energy is dissipated so that the emitted light photons are of lower energy than those absorbed. One of such most familiar phenomenon is fluorescence, which has a short lifetime (10^{-8} to 10^{-4}s)[67].

2.2.2.3 Phosphorescence

Phosphorescence is a radiational transition, in which the absorbed energy undergoes intersystem crossing into a state with a different spin multiplicity. The lifetime of phosphorescence is usually from 10^{-4} - 10^{-2} s, much longer than that of Fluorescence. Therefore, phosphorescence is even rarer than fluorescence, since a molecule in the triplet state (Figure 25) has a good chance of undergoing intersystem crossing to ground state before phosphorescence can occur[67].

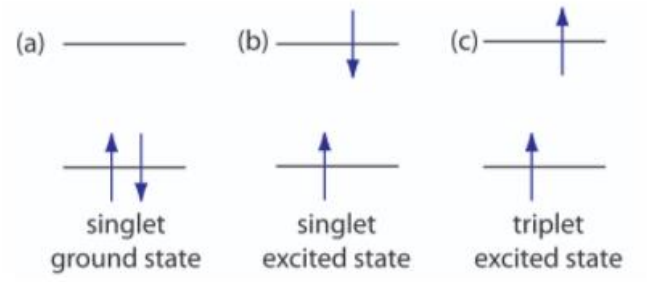

Figure 26: Electron configurations for (a) a singlet ground state, (b) a singlet excited state and (c) a triplet excited state[69].

2.2.3 Typical PL spectrometer components

2.2.3.1 Light Sources

A light source is needed in order to provide the excitation light witch will excite the sample. A light source can be: A laser, Arc and Incandescent Xenon Lamps, High Pressure Mercury Lamps, Xe-Hg Arc Lamps, Low Pressure Hg and Hg-Ar Lamps and other light Sources like pulsed xenon lamps, quartz-tungsten halogen (QTH) lamps, LED light sources, etc[67].

2.2.3.2 Monochromators

Most of the light sources used to provide only polychromatic or white light. However, what is needed for experiments are various chromatic light with a wavelength range of 10 nm. Monochromators help us to achieve this aim. Prisms and diffraction gratings are the two main kinds of monochromators used, although diffraction gratings are most useful, especially in spectrofluorometers[67].

Dispersion, efficiency, stray light level and resolution are important parameters for monochromators. Dispersion is mainly determined by slit width and expressed in nm/mm. It is prepared to have low stray light level. Stray light is defined as light transmitted by the

monochromator at wavelength outside the chosen range. Also, a high efficiency is required to increase the ability to detect low light levels. Resolution depends on the slit width. There are normally two slits, entrance and exit in a fluorometers. Light intensity that passes through the slits is proportional to the square of the slit width. Larger slits have larger signal levels, but lower resolution, and vice versa. Therefore, it is important to balance the signal intensity and resolution with the slit width[67].

2.2.3.2 Optical filters

Optical filters are used in addition to monochromators, because the light passing through monochromator is rarely ideal, optical filters are needed for further purifying light source. If the basic excitation and emission properties of a particular system under study, then selectivity by using optical filters is better than by the use of monochromators. Two kinds of optical filter are gradually employed: colored filters and thin-film filters[67].

Colored Filters: Colored filters are the most traditional filter used before thin-film filter were developed. They can be divided into two categories: monochromatic filter and long-pass filter. The first one only passes a small range of light (about 10 - 25 nm) centered at particular chosen wavelength. In contrast, long pass filter transmits all wavelengths above a particular wavelength. In using these bandpass filters, special attention must be paid to the possibility of emission from the filter itself, because many filters are made up of luminescent materials that are easily excited by UV light. In order to avoid this problem, it is better to set up the filter further away from the sample[67].

Thin-film Filters: The transmission curves of colored class filter are not suitable for some application and as such they are gradually being substituted by thin-film filters. Almost any desired transmission curve can be obtained using a thin film filter[67].

2.2.3.3 Detectors

The standard detector used in many spectrofluorometers is the InGaAs array, which can provide rapid and robust spectral characterization in the near-IR. And the liquid-nitrogen cooling is applied to decrease the background noise. Normally, detectors are connected to a controller that can transfer a digital signal to and from the computer[67].

A typical Luminescence spectrometer setup is shown in Figure 27:

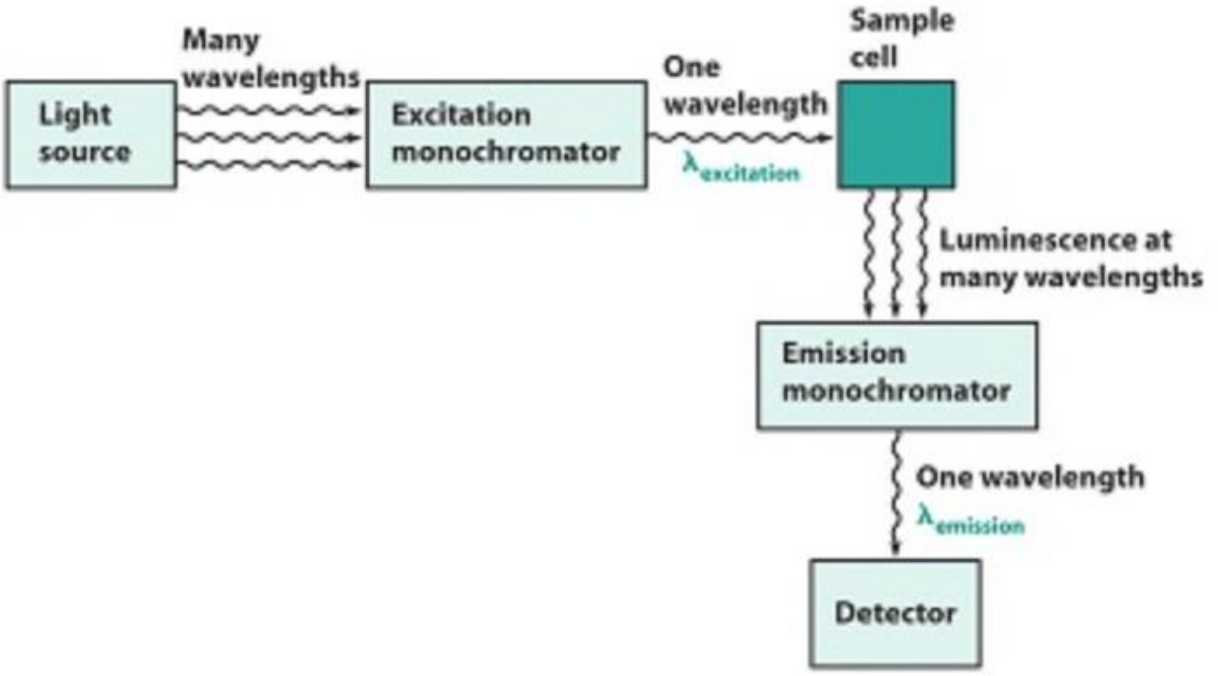

Figure 27: A Photoluminescence spectrometer consisting of a light source, excitation monochromator, sample cell, emission monochromator and a detector.

2.3 Scanning Electron Microscopy (SEM)

Scanning electron microscopy (SEM), which is also recognized as SEM analysis or SEM technique, has been used worldwide in many disciplines. The main difference between the SEM and other microscopy techniques is that the SEM utilizes an accelerated electron beam instead of light and also depends upon electron emission. It can be regarded as an effective method in analysis of organic and inorganic materials on a nanometer to micrometer (µm) scale. SEM works at a high magnification reaches to 300,000x and even 1000000 (in some modern models) in producing images very precisely of wide range of materials. Energy Dispersive X-ray Spectroscopy (EDS) works together with SEM to provide qualitative and semi-quantitative results. Both techniques, together, have the potential to introduce fundamental information on material composition of scanned specimens, which could not be provided by the common laboratory tests[70].

2.3.1 Principles of Scanning Electron Microscopy (SEM)

Accelerated electrons in an SEM carry significant amounts of kinetic energy, and this energy is dissipated as a variety of signals produced by electron-sample interactions when the incident electrons are decelerated in the solid sample. These signals include secondary electrons (SE) that produce SEM images, backscattered electrons (BSE), diffracted backscattered electrons (EBSD) that are used to determine crystal structures and orientations of minerals, photons (characteristic X-rays) that are used for elemental analysis and continuum X-rays, visible light, and heat[71].

Secondary electrons and backscattered electrons are commonly used for imaging samples: secondary electrons are most valuable for showing morphology and topography on samples and backscattered electrons are most valuable for illustrating contrasts in composition in multiphase samples. X-ray generation is produced by inelastic collisions of the incident electrons with electrons in discrete orbitals (shells) of atoms in the sample. As the excited electrons return to lower energy states, they yield X-rays that are of a fixed wavelength (that is related to the difference in energy levels of electrons in different shells for a given element). Thus, characteristic X-rays are produced for each element in a mineral that is "excited" by the electron beam. SEM analysis is considered to be "non-destructive"; that is, x-rays generated by electron interactions do not lead to volume loss of the sample, so it is possible to analyze the same materials repeatedly[71].

Electrons accelerated onto a material result in a number of interactions with the atoms of the target sample. Accelerated electrons can pass through the sample without interaction, undergo elastic scattering and can be inelastically scattered. Elastic and inelastic scattering result in a number of signals that are used for imaging, quantitative and semi-quantitative information of the target sample and generation of an X-ray source. Typical signals used for imaging include secondary electrons (SE), backscattered electrons (BSE), cathodoluminescence (CL), auger electrons and characteristic X-rays. Quantitative and semiquantitative analyses of materials as well as element mapping typically utilize characteristic X-rays. Bremsstrahlung (continuum) radiation is a continuous spectrum of X-rays from zero to the energy of the electron beam, and forms a background in which characteristic X-ray must be considered. Further, X-rays generated from a specific target material are used as the roughly fixed-wavelength energy source for X-ray diffraction (XRD) and X-ray fluorescence (XRF) investigations[71]. All these interactions between the incident electron beam and the sample can be seen in Figure 28.

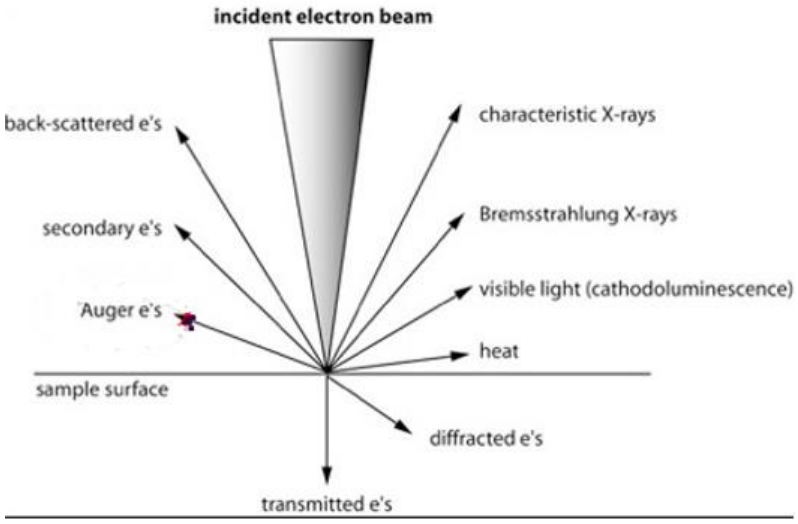

Figure 28: Incident electron beam-Sample interactions[71].

Where an electron beam impinges on a sample, electron scattering and photon- and X-ray-production develops in a volume (the electron interaction volume, Figure 29) that is dependent on several factors. These include[71]:

- The energy of the incident beam (accelerating potential) increases the interaction volume, but decreases the elastic scattering (e.g. backscattering).
- The interaction volume decreases as a function of the mean atomic weight.
- Smaller and more asymmetric interaction volumes develop in samples tilted relative to the impinging electron beam.

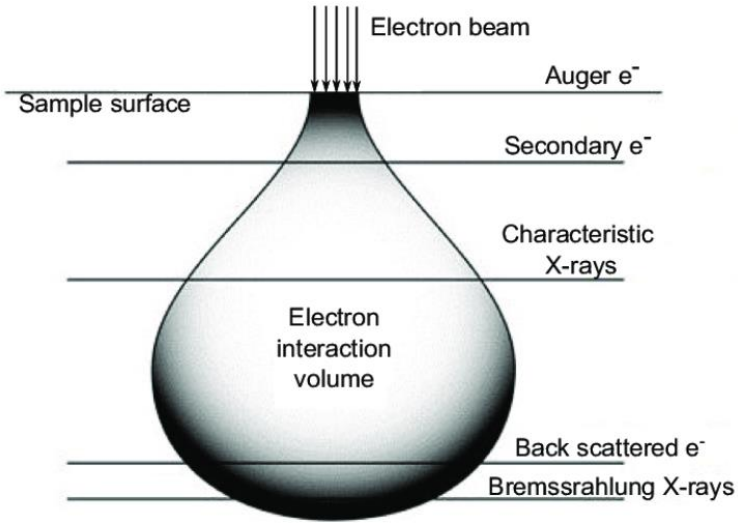

Figure 29: Electron beam interaction volume[72].

Each of the signals used for imaging or X-ray generation is generated from different electron interaction volumes and, in turn, each of the signals has different imaging or analytical resolution. Auger and Secondary images have the best imaging resolution, being generated in the smallest volume near the surface of the sample. Backscattered electrons are generated over a larger volume resulting in images of intermediate resolution. Cathodoluminescence is generated over the largest volume, even larger than Bremsstrahlung radiation, resulting in images with the poorest resolution[71].

2.3.3 Important SEM components and functionality

A typical SEM setup with its components is shown below.

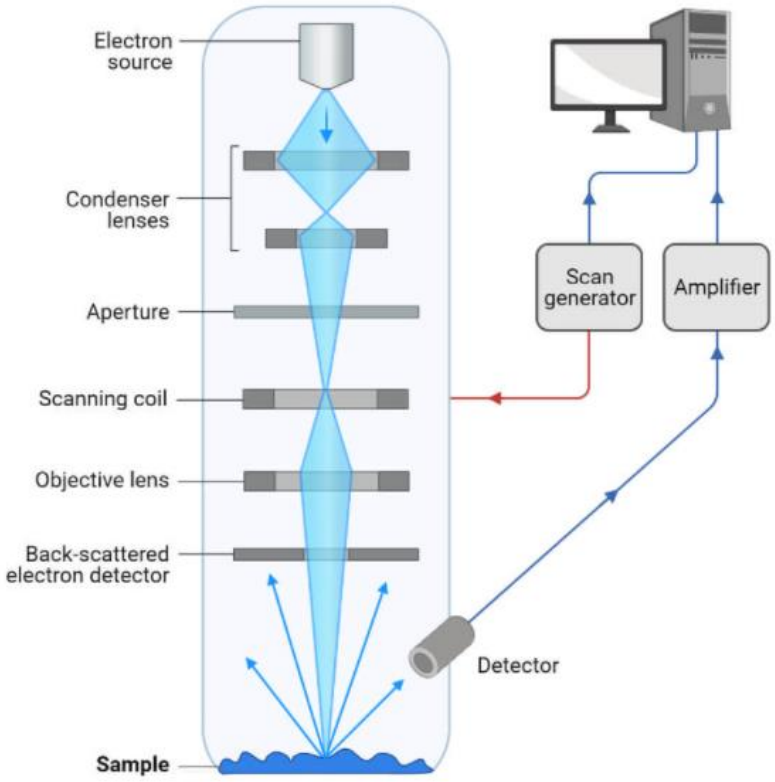

Figure 30: A typical SEM setup[73].

2.3.3.1 How the SEM works

- The source of the electrons and the electromagnetic lenses are from tungsten filament lamps that are placed at the top of the column.
- The electrons are emitted after thermal energy is applied to the electron source and allowed to move in a fast motion to the anode, which has a positive charge.
- The beam of electrons activates the emission of primary scattered (Primary) electrons at high energy levels and secondary electrons at low-energy levels from the specimen surface. The beam of electrons interacts with the specimen to produce signals that give information about the surface topography and composition of the specimen.
- The specimen does not need special treatment for visualization under the SEM, even air-dried samples can be examined directly. However, microbial specimens need fixation, dehydration, and drying in order to maintain the structural features of the cells and to prevent collapsing of the cells when exposed to the high vacuum of the microscope.
- The samples are mounted and coated with thin layer of heavy metal elements to allow spatial scattering of electric charges on the surface of the specimen allowing better image production, with high clarity.
- Scanning by this microscope is attained by tapering a beam of electrons back and forth over a thin section of the microscope. When the electrons reach the specimen, the surface releases a tiny staw of electrons known as secondary electrons which are then trapped by a special detector apparatus.
- When the secondary electrons reach and enter the detector, they strike a scintillator (a luminescence material that fluoresces when struck by a charged particle or high-energy photon). This emits flashes of light which get converted into an electric current by a photomultiplier, sending a signal to the cathode ray tube. This produces an image that looks like a television picture that can be viewed and photographed.
- The quantity of secondary electrons that enter the detector is highly defined by the nature of the specimen i.e raised surfaces to receive high quantities of electrons, entering the detector while depressed surfaces have fewer electrons reaching the surface and hence fewer electrons enter the detector.
- Therefore, raised surfaces will appear brighter on the screen while depressed surfaces appear darker.

2.3.3.2 The major components of the Scanning Electron Microscope

Electron Source: This is where electrons are produced under thermal heat at a voltage of 1-40kV. the electrons condense into a beam that is used for the creation of an image and analysis. There are three types of electron sources that can be used i. e Tungsten filament, Lanthanum hexaboride, and Field emission gun (FEG)[73].

Lenses: It has several condenser lenses that focus the beam of electrons from the source through the column forming a narrow beam of electrons that form a spot called a spot size[73].

Scanning Coil: They are used to deflect the beam over the specimen surface[73].

Detector: It's made up of several detectors that are able to differentiate the secondary electrons, backscattered electrons, and diffracted backscattered electrons. The functioning of the detectors highly depends on the voltage speed, the density of the specimen[73].

Chapter 3: Experimental methods and Results

3.1 Synthesis and properties of silver metaphosphate ($AgPO_3$) glass

The silver metaphosphate glass is an ideal host-matrix for many materials due to its soft nature which is a consequence of its low transition temperature (T_g=190 °C) allowing the easy incorporation of many materials. Another reason why the $AgPO_3$ is attractive, is that its vey easy to produce, has low production cost, and is also non-toxic. Another property of the glass, is that is transparent to most of the visible light, and has no crystallinity (Figure 31) .

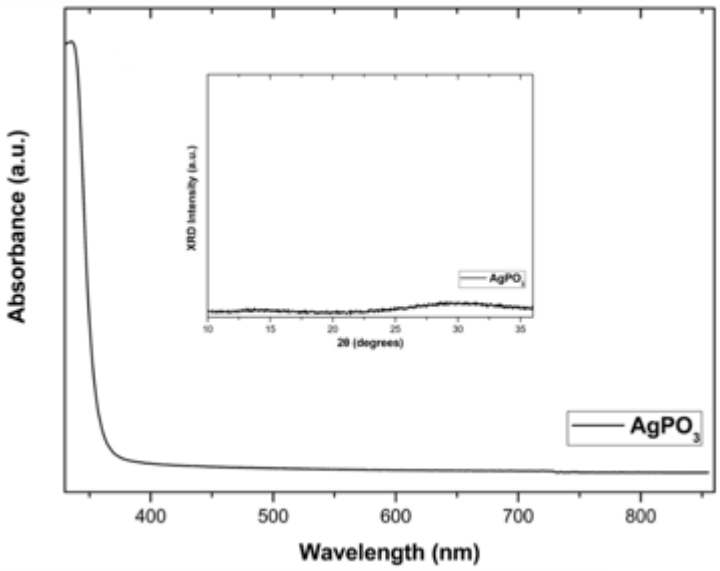

Figure 31: Optical Absorbance of the $AgPO_3$ glass (Inset: XRD of the $AgPO_3$ glass showing no peak and thus no crystallinity).

For the synthesis of the silver metaphosphate glass ,equimolar amounts of high purity dry powders of Ammonium Dihydrogen Phosphate ($NH_4H_2PO_4$) (purity: 99.999%) and Silver Nitrate ($AgNO_3$) (purity: 99.995%) were mixed in a platinum crucible. All weighting and mixing manipulations of the powders were carried out within a glove purged by dry nitrogen gas. Then, the melting batch was transferred in an electrical furnace initially held at 170 °C. The temperature was slowly increased to 290 °C for the smooth evaporation of the volatile gas products. The furnace temperature then, was raised in 450 °C and kept steady for 30 minutes, while performing regular stirring in order to ensure melt homogeneity. Immediately after removing the crucible from the furnace, the melted batch was poured carefully on a Si substrate, then immediately got splat-quenched with another Si substrate. After some seconds in order for the glass to cool down, $AgPO_3$ glasses were obtained in the form of 1 mm thick disk specimens with a diameter of around

10 mm, upon splat-quenching the melt between two Si substrates[9]. This procedure is schematically illustrated in Figure 32.

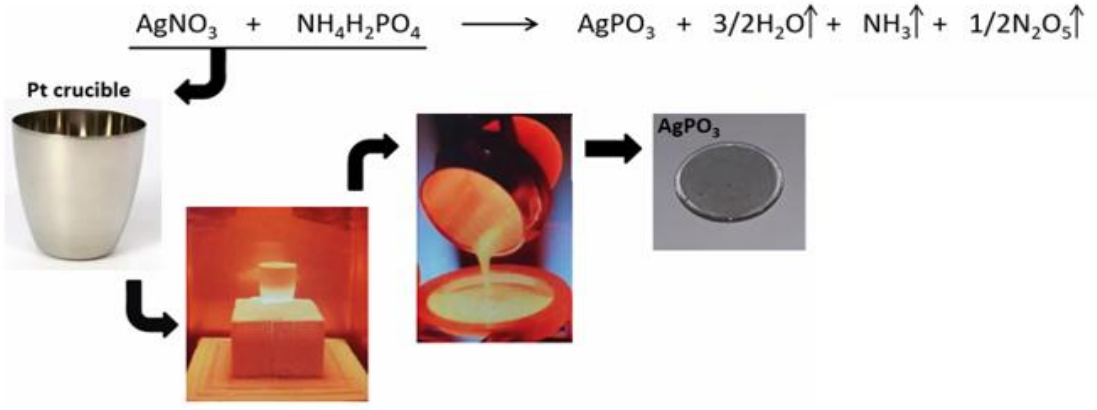

Figure 31: Synthesis of Silver metaphosphate glass

3.2 Exfoliation and properties of Molybdenum Disulfide (MoS_2) flakes

MoS_2 fakes were prepared from bulk MoS_2 powder (grain size<2 µm, Sigma Aldrich) using liquid phase exfoliation (LPE) method, as reported elsewhere. In detail, 40 mg of bulk MoS_2 powder was dissolved in 10 ml IPA. The solution was ultrasonicated for 60 min in a Elma S 30 H bath sonicator (Elma Schmidbauer GmbH, Germany) under 80 W power and 37 kHz frequency. Room temperature (<30 °C) was maintained throughout the exfoliation process. After ultrasonication the dispersion was centrifuged to exclude the unexfoliated bulk MoS_2 [9]. The lateral dimension of the flakes came out to be 1µm and the average thickness is around 4nm (Figure 32).

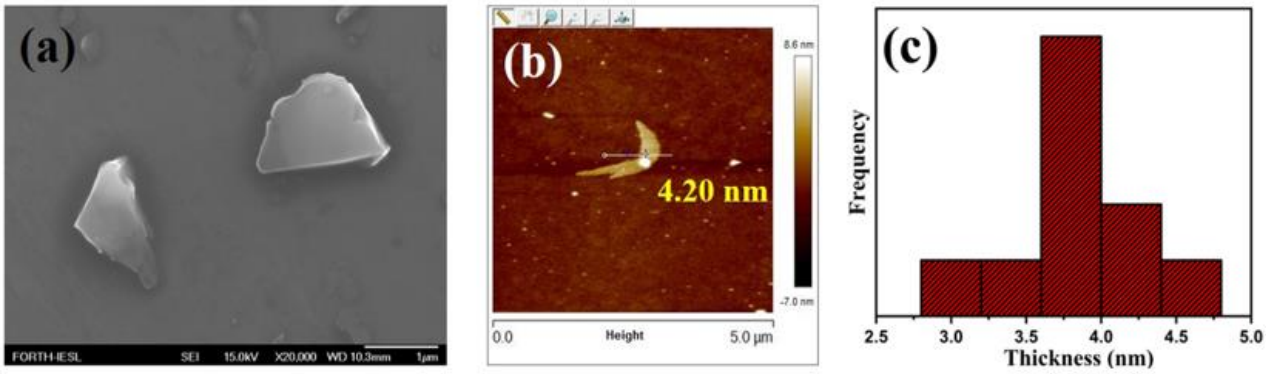

Figure 32: a) SEM image of two MoS_2 flakes on a Si substrate, b) Atomic force microscopy image of a MoS_2 flake and c) Thickness distribution of MoS_2 [9].

3.3 Development of $AgPO_3$:MoS_2 nano-heterojunctions

For the incorporation of MoS_2 (Figure 32), the $AgPO_3$ glass substrate was positioned on a silicon wafer while a heating plate was employed in order to maintain a temperature around 80 °C. Ten drops of a previously prepared MoS2 solution (0.76 mg/ml) were drop-casted on the surface of the $AgPO_3$ glass, while allowing 10 s intervals between each drop in order to ensure smooth solvent vaporization. After solvent removal the residual MoS_2 fakes were randomly distributed on the $AgPO_3$ surface. Then, the temperature was raised to 170 °C for 2 min, i.e. 22 °C below the glass transition temperature of the $AgPO_3$ glass. At this temperature, the $AgPO_3$ glass becomes viscous and allows readily the smooth incorporation of the MoS_2 fakes within the glass matrix. Following MoS_2 immersion, the $AgPO_3$:MoS_2 nano-hybrid glass was splat-quenched between two silicon wafers, while instantly removed from the heating plate and left to cool down to room temperature. The employment of silicon wafers allows the formation of smooth surfaces on both sides of the composite glass specimens and renders them suitable for optical characterization[9].

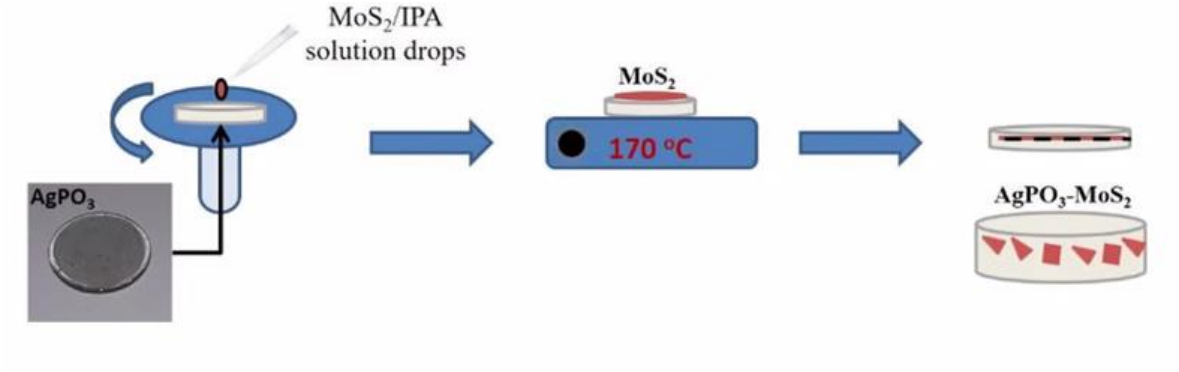

Figure 33: Schematic illustration of the incorporation procedure of exfoliated MoS_2 flakes.[9]

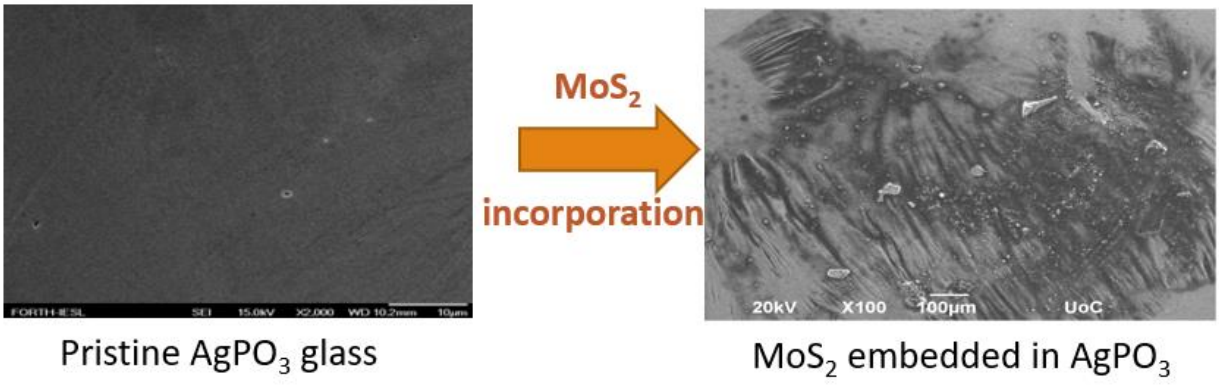

Figure 34: SEM images of a $AgPO_3$ glass before and after incorporation of the MoS_2 flakes.

3.4 Experimental results and interpretation

After the incorporation process, using a femtosecond laser LIPSS were created on the $AgPO_3$:MoS_2 glass surface. Using different step laser parameters, two different LIPSS regions were created. SEM images of these regions are shown below in Figure 35.

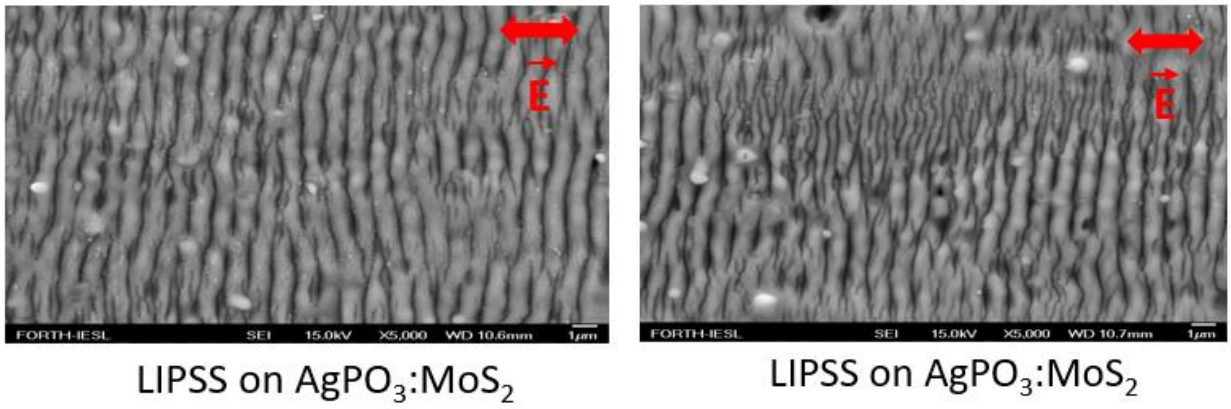

Figure 35: SEM images of the LIPSS regions **A)** (right) and **B)** (left).

The region on the right will be called **Region A)** and that on the left **Region B)**. Region **A)** formed under laser power 30mW, Step 10μm and scanning speed 1mm/s, while keeping the Z distance steady at 10cm (the distance between the laser and the sample). Region **B)** was formed under Laser power 30mw, step 15μm and scanning speed at 1mm/s with the same Z. As it is shown, the ripples on the glass surface are formed perpendicular to the laser's electric field polarization as expected by the Sipe model. One the other hand It was also expected to see the embedded MoS_2 flakes resurface and stay on top and between of the LIPSS. Thus, it was suspected that the MoS_2 is ablated upon irradiation with the femtosecond laser. In order to further shed light upon this observation, Raman and PL spectra of these region were obtained.

As shown in Figure 35, Raman spectra of a Pristine $AgPO_3$ (dark curve), $AgPO_3$:MoS_2 (blue curve), and a $AgPO_3$:MoS_2 patterned region (red curve) was obtained. From the Raman spectra of the pristine $AgPO_3$ we see two clear and distinct peaks, these peaks correspond to the symmetric stretching vibration of the P-O-P bridges (V_s P-O-P) at 681.82 cm^{-1} and the symmetric stretching vibration of the terminal phosphate groups (V_s PO_2) at 1133.57 cm^{-1}. From the spectra of the $AgPO_3$:MoS_2 we see four peaks, the two peaks of the metaphosphate glass that were just mentioned, and two new peaks corresponding to the in-plane (E_{2g}) and out of plane (A_{1g}) vibrational modes of the 2H-phase MoS_2 crystal at 383.39 cm^{-1} and 409.43 cm^{-1} respectively. Finally, form the spectra of the $AgPO_3$:MoS_2 we see the two well-known peaks of the metaphosphate glass, but the Raman modes of the MoS_s are absent. This data, along with the PL spectra (Figure 36) of the patterned regions **A)** and **B)** from which we see a typical $AgPO_3$ background and not the A and B exciton peaks is a strong indication that the MoS_2 is ablated upon irradiation from the femtosecond laser.

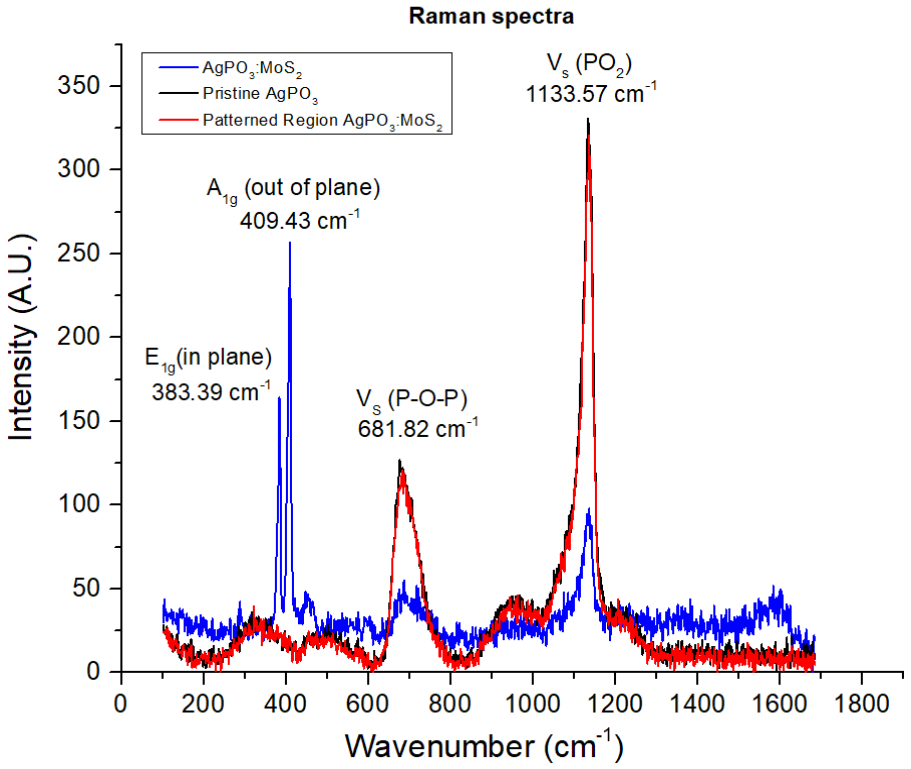

Figure 35: Raman spectra of the $AgPO_3$ (black), $AgPO_3$:MoS_2 (blue) and a patterned region of $AgPO_3$:MoS_2 (red).

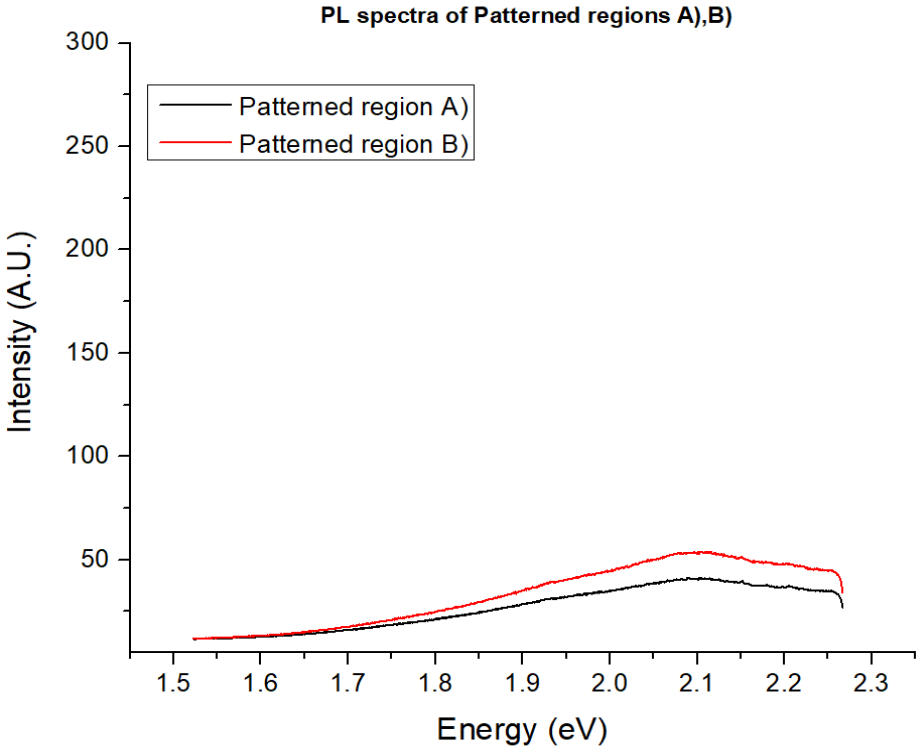

Figure 36: Photoluminescence spectra of **A)** and **B)** patterned regions

In order to overcome this obstacle, the decision to drop-cast MoS_2 flakes on top of the patterned regions was made. SEM images of before/after the drop-cast of the MoS_2 are shown below. **A)** Region is shown on the right column and **B)** on the left column.

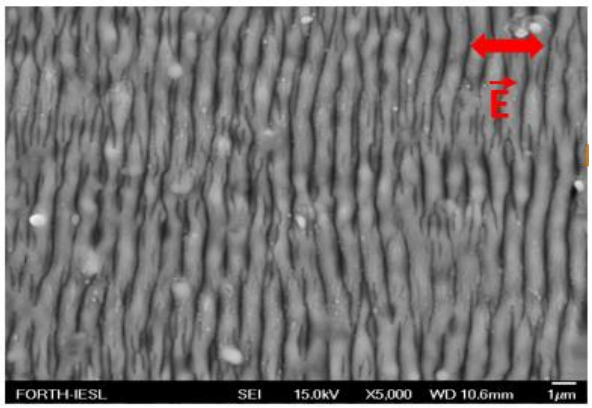

LIPSS on $AgPO_3$:MoS_2

MoS_2 Drop Cast

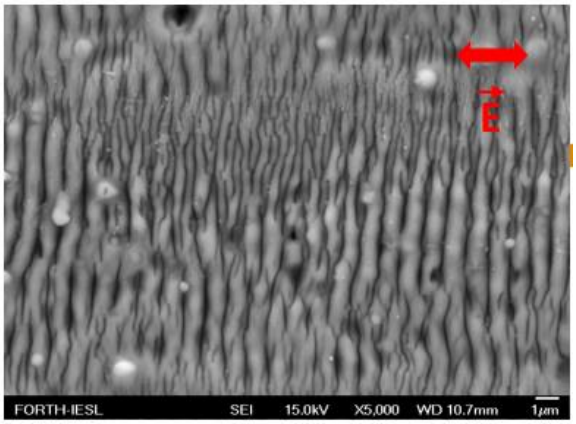

LIPSS on $AgPO_3$:MoS_2

MoS_2 Drop Cast

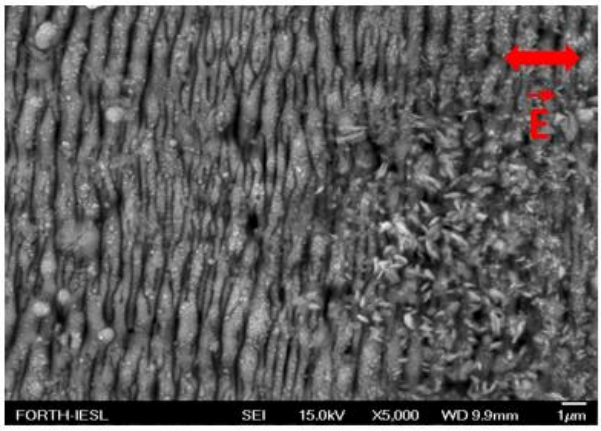

MoS_2 on top of LIPSS

Zoom

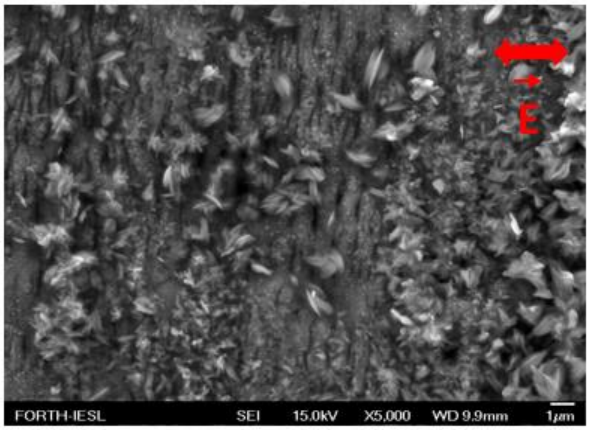

MoS_2 on top of LIPSS

Zoom

MoS_2 on top of LIPSS under zoom

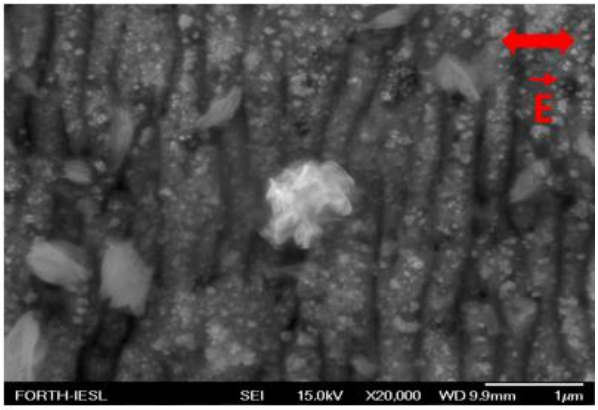

MoS_2 on top of LIPSS under zoom

The next step was to measure the Raman spectra of the regions **A)** and **B)** and see how the strain of the LIPSS applied on the few-layered MoS_s flakes effects the PL properties of the 2D material. The Raman spectra are shown below.

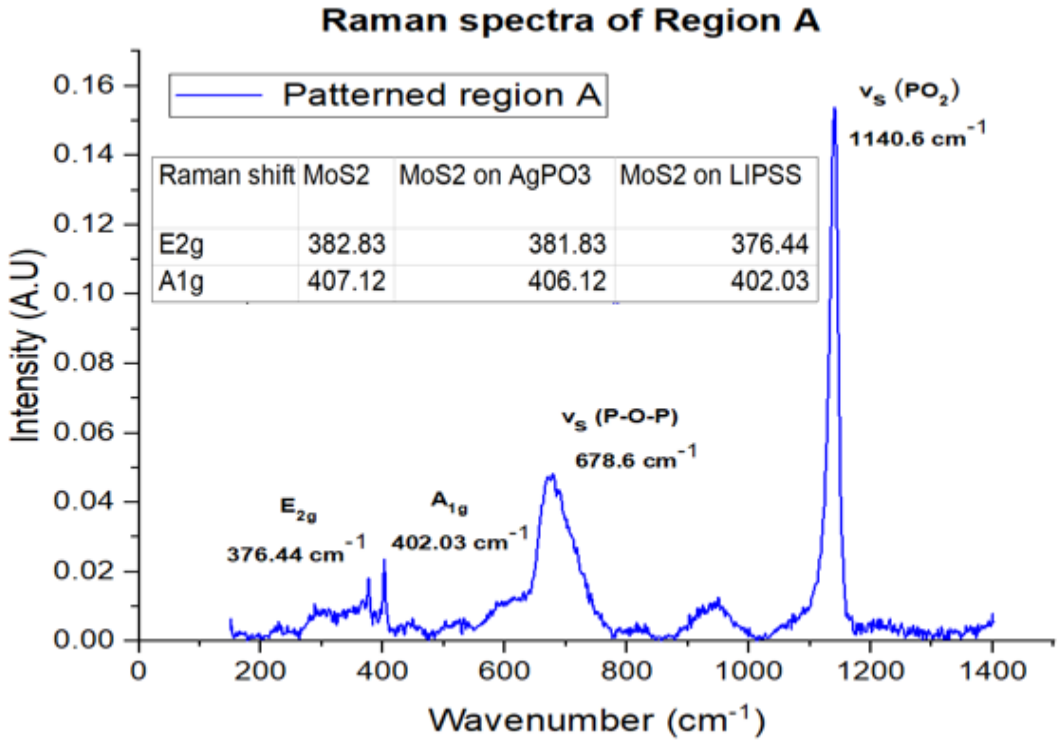

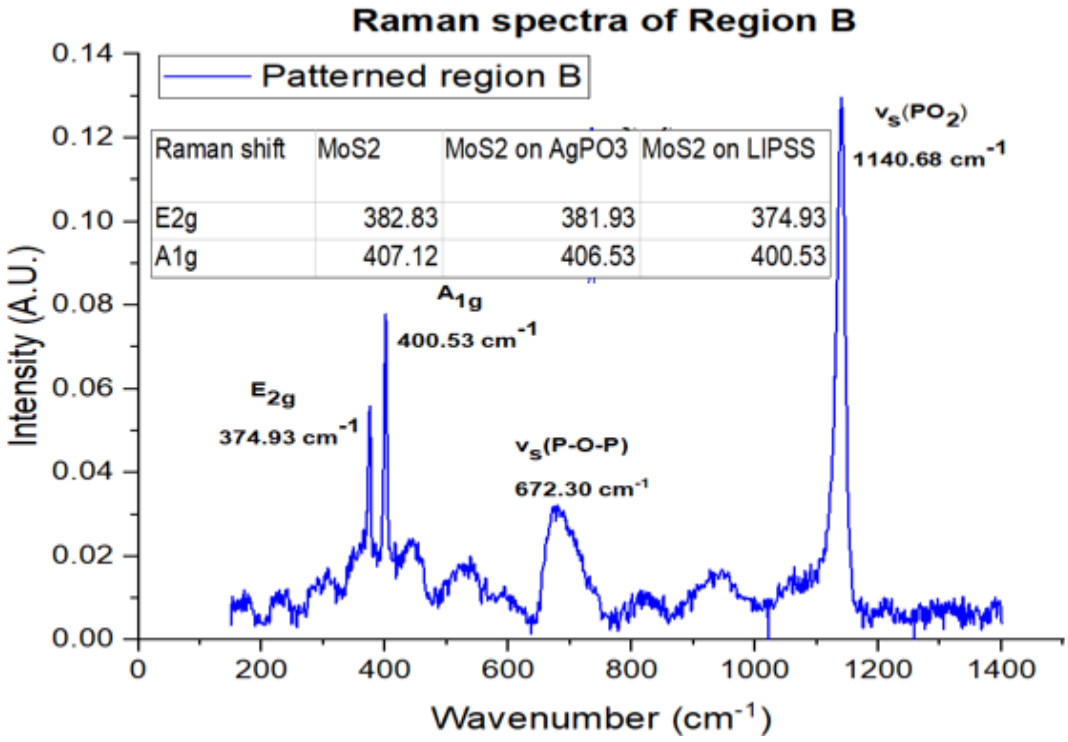

From the Raman spectra shown above we are able to observe both in **A)** and **B)** regions the peaks associated with the vibrational modes of the $AgPO_3$ glass and the MoS_2. More specifically for the **A)** region we observe the symmetric stretching vibration of the P-O-P bridges (V_s P-O-P) at 678.60 cm^{-1} and the symmetric stretching vibration of the terminal PO_2 groups (Vs PO_2) at 1140.60 cm^{-2}. The two Raman modes of the MoS_2, in-plane (E_{2g}) and out of plane (A_{1g}) are observed at 376.44 cm^{-1} and 402.03 cm^{-1} respectively. Now for the **B)** region we observe the V_s P-O-P at 672.30 cm^{-1} and the V_s PO_2 at 1140.68 cm^{-1} and the vibrations of MoS_2 E_{2g} and A_{1g} at 374.93 cm^{-1} and 400.43 cm^{-1} respectively.

It is well known, that strain effect can force shifts on the Raman modes of the material when it is applied [74]. The strain, when applied, changes the lattice constant of the material's crystal structure and as a result, Raman shift is observed. Also, it is possible to observe a split of the Raman modes as a result of strain. However, we do not observe something similar in our spectra. Left shift indicates tensile strain or increase in the lattice constant. Right shift indicates compressive strain or decrease in the lattice constant. As an inset in both Raman spectra, a table comparing how the peaks of the vibrational modes of the MoS_2 change upon putting the material on top of the $AgPO_3$ without any LIPSS performed and upon putting the material on top of a $AgPO_3$ region with LIPSS in comparison to the bare MoS_2 vibrational modes. We observe a small change in the wavenumber $\Delta K \sim 1$ cm^{-1} of both the E_{2g} and A_{1g} upon putting the MoS_s flakes on the pristine $AgPO_3$ surface. Now, as of the **A)** region we observe a 5.39 cm^{-1} left shift of the E_{2g} mode and a 4.09 cm^{-1} left shift of the A_{1g} mode. In the case of the **B)** region, we observe a 6.9 cm^{-1} left shift of the E_{2g} mode and a 5.59 cm^{-1} left shift of the A_{1g} vibrational mode. Thus, it is safe to conclude that a strain effect is indeed applied in the MoS_2 flakes.

For the final measurement of this project, the PL spectra of the strained MoS_2 flakes for both A) and B) regions is obtained. Three curves are shown in each spectrum of **A)** and **B)** regions. The curves with the color blue and red correspond to two different spots in each patterned region. The black curve corresponds to the PL spectra obtained from a spot with the MoS_s embedded in the $AgPO_3$ as a reference spectrum. Both spectra are shown in page 49.

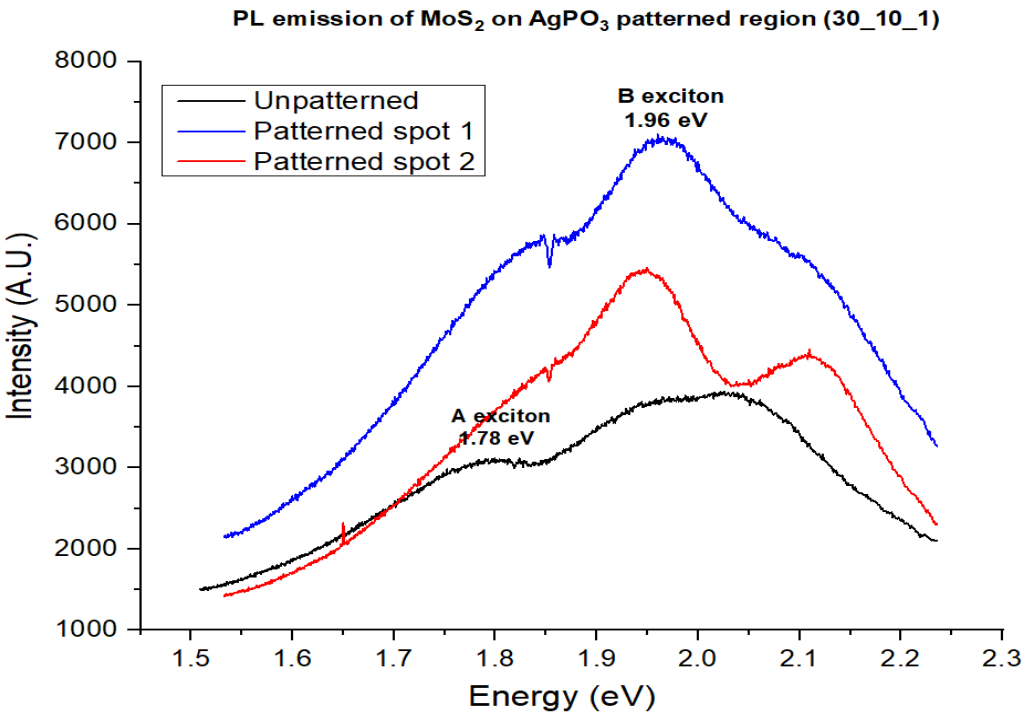

Figure 37: PL spectra of the **A)** region

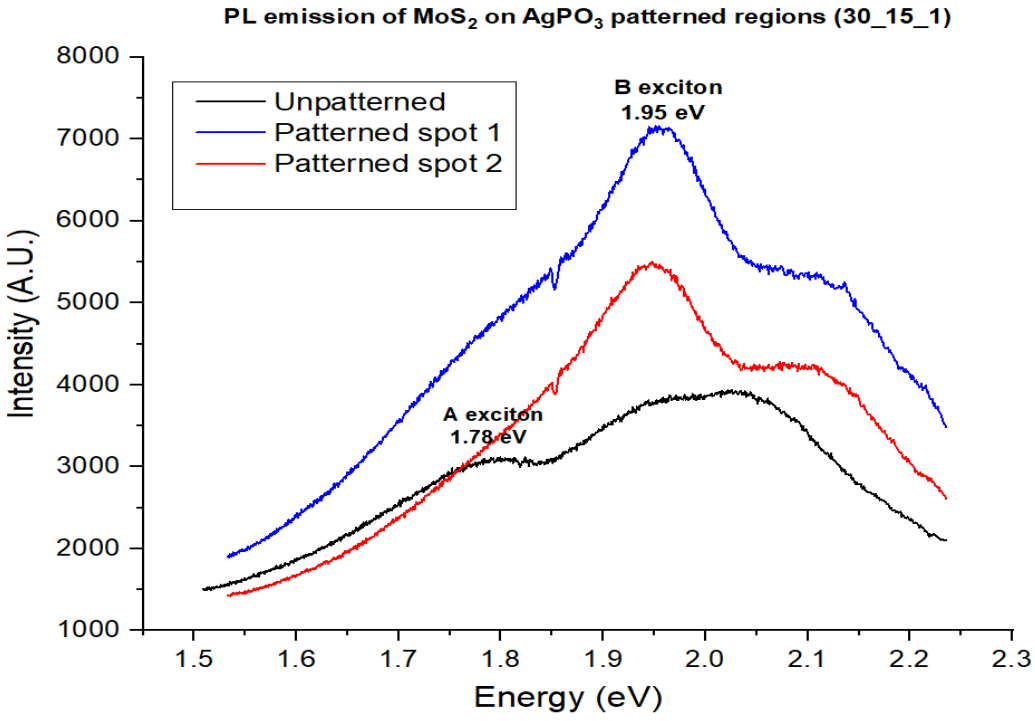

Figure 38: PL spectra of the **B)** region

In the PL spectra of the region **A)** we observe a strong and distinct B-exciton emission at 1.96eV compared to that of the MoS_2 embedded in the $AgPO_3$. Also, we observe an enhanced A exciton emission at 1.78eV compared to the $AgPO_3$:MoS_2 curve. Additionally, a third strong peak between the range of the 2.1-2.2 eV is observed in both reference and patterned spots curves. This pick could be attributed to impurities. We are having the same situation in the PL spectra of the region **B)**, a strong B-exciton emission is also observed at 1.95eV, but the A exciton peak is not so clear and distinct, however its peak is at 1.78eV. A third peak around 2.1-2.2 eV is also present.

For an attempt to give an interpretation on the enhanced A and B exciton emission observed we must look at the exciton-plasmon coupling mechanism and also, how the strain can help make these emissions stronger. From the exciton plasmon coupling point of view, there are two effects taking place i) the effective dipole-dipole interaction between the the exciton and the plasmon and ii) a fast charge transfer from the MoS_2 to the $AgPO_3$. These effects are antagonistic and lead to the observed enhancement (Figure 39) [9].

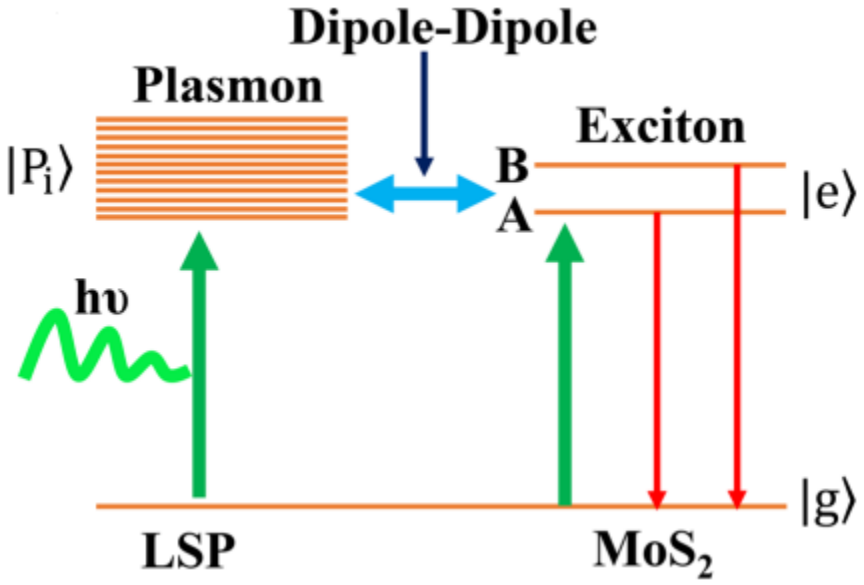

Figure 39: The exciton-plasmon coupling mechanism[9]

From the strain point of view, in order to understand the PL enhancement quantitively the occupancy at the direct CB valleys at the K-points in the K-Space (also called reciprocal space) must be considered (for A and B exciton emissions separately) as show in Figure 39 on page 51.

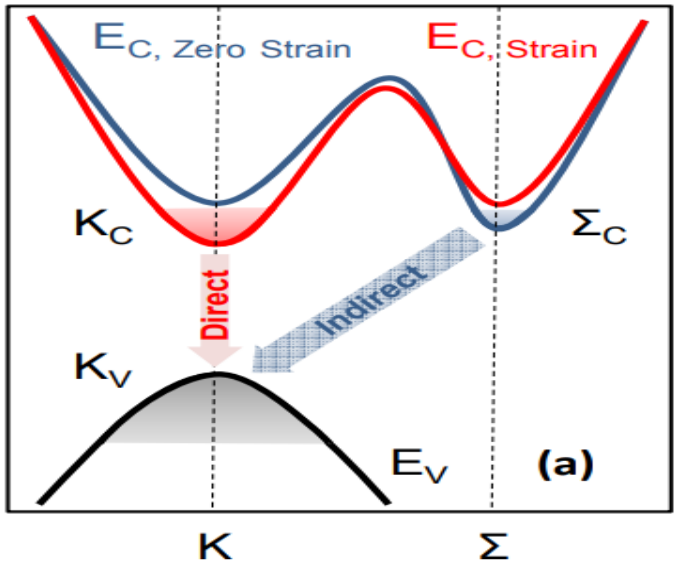

Figure 40: Bandgap changed under strain

It has been demonstrated that the strain can change the bandgap of the material[74]. As shown in Figure 40, tensile strain changes the CB minima, with the direct CB valleys Kc moving down while the indirect CB valleys Σc moving up in energy, also the difference between the Kc – Σc points in the reciprocal space is reducing. As a result, the occupancy of electrons in each valley correspondingly changes with strain. As the Kc - Σc difference reduces with increasing strain, the PL increases drastically resulting in the two peaks merging[74].

Conclusions

In this project we utilized a nano heterojunction system consisting of few-layered MoS_2 flakes embedded in a $AgPO_3$ matrix. The aim of the project was to combine the effect of the exciton-plasmon coupling with a strain effect induced from the LIPSS created by a femtosecond laser. Our aim was to try and enhance the photoluminescence properties of few-layered MoS_2 and more specifically the B-Exciton emission at room temperature. We started by embedding the MoS_2 flakes below the glass surface, then using a femtosecond laser, two regions **A)** and **B)** with different laser parameters were created. However, after irradiation the embedded flakes were ablated as it was confirmed by both Raman and PL measurements that were carried out, and this led to an alternative method which was to drop-cast the MoS_2 flakes on top of the LIPSS. After Raman measurements of both the **A)** and **B)** regions, we observed left shifted Raman peaks compared to the peaks of the MoS_2 flakes on top of the $AgPO_3$ glass. This was a clear indication of the strain effect applied on the 2D material. In addition, the peaks of the $AgPO_3$ were unchanged compared to the pristine glass, meaning that this process indeed did not change the glass structure. The PL measurements were the next to be obtained. From the PL spectra of both **A)** and **B)** regions we observed strong and distinct B-exciton emission indicating that the strain effect has indeed enhanced the B-exciton. However, the A-exciton emission was distinct only in region **A)**. Finally, a third peak around 2.1-2.2 eV was observed, but its roots were unidentified. Taking all the above into account, this project is an example of the remarkable optical properties that makes the TMDs so appealing for their use in optoelectronic applications. Controlling the A and B exciton emissions for example, could give us the capability to be able to choose the operating wavelength of a device based on TMDs. However, a more systematic work needs to be done, in order to further shed light on how the periodicity of the LIPSS affects the strain profile and how the different strain profiles, in turn, affects the photoluminescence properties of the few-layered MoS_2.

References

1. Difference Between Valence Band and Conduction Band (with Comparison Chart) - Circuit Globe, (2021).

2. R. Pashotta, (2008).

3. Valence and conduction bands - Wikipedia, (n.d.).

4. G. Sun, Advances in Optics and Photonics **3**, 53 (2011).

5. K. S. Novoselov, D. Jiang, F. Schedin, T. J. Booth, V. v. Khotkevich, S. v. Morozov, and A. K. Geim, Proceedings of the National Academy of Sciences **102**, 10451 (2005).

6. F. Schwierz, Nature Nanotechnology 2011 6:3 **6**, 135 (2011).

7. R. Ganatra and Q. Zhang, ACS Nano **8**, 4074 (2014).

8. K. F. Mak, C. Lee, J. Hone, J. Shan, and T. F. Heinz, Physical Review Letters **105**, 136805 (2010).

9. Abdus S. Sarkar, Robust B-exciton Emission at Room Temperature in Few-layers of MoS2:Ag Nanoheterojunctions Embedded into a Glass Matrix (2020).

10. S. Manzeli, D. Ovchinnikov, D. Pasquier, O. v. Yazyev, and A. Kis, Nature Reviews Materials 2017 2:8 **2**, 1 (2017).

11. B. Radisavljevic, A. Radenovic, J. Brivio, V. Giacometti, and A. Kis, Nature Nanotechnology **6**, 147 (2011).

12. A. Splendiani, L. Sun, Y. Zhang, T. Li, J. Kim, C. Y. Chim, G. Galli, and F. Wang, Nano Letters **10**, 1271 (2010).

13. H. M. Hill, A. F. Rigosi, K. T. Rim, G. W. Flynn, and T. F. Heinz, Nano Letters **16**, 4831 (2016).

14. Z. Y. Zhu, Y. C. Cheng, and U. Schwingenschlögl, Physical Review B - Condensed Matter and Materials Physics **84**, (2011).

15. A. Kormányos, G. Burkard, M. Gmitra, J. Fabian, V. Zólyomi, N. D. Drummond, and V. Fal'ko, 2D Materials **2**, 022001 (2015).

16. D. Xiao, G. bin Liu, W. Feng, X. Xu, and W. Yao, Physical Review Letters **108**, (2012).

17. A. Pulkin and O. v. Yazyev, Physical Review B **93**, (2016).

18. T. Habe and M. Koshino, Physical Review B - Condensed Matter and Materials Physics **91**, (2015).

19. A. v. Kolobov and J. Tominaga, Springer Series in Materials Science **239**, 321 (2016).

20. A. Steinhoff, M. Florian, A. Singh, K. Tran, M. Kolarczik, S. Helmrich, A. W. Achtstein, U. Woggon, N. Owschimikow, F. Jahnke, and X. Li, Nature Physics **14**, 1199 (2018).

21. M. Tebyetekerwa, J. Zhang, Z. Xu, T. N. Truong, Z. Yin, Y. Lu, S. Ramakrishna, D. Macdonald, and H. T. Nguyen, ACS Nano **14**, 14579 (2020).

22. Plasmon - Wikipedia (n.d.).

23. E. Cao, W. Lin, M. Sun, W. Liang, and Y. Song, Nanop **7**, 59 (2018).

24. Physics and Radio-Electronics, (2015).

25. J. E. Sipe, J. F. Young, J. S. Preston, and H. M. van Driel, Physical Review B **27**, 1141 (1983).

26. J. Z. P. Skolski, (2014).

27. J. E. S. and J. F. Young. L. coherent modulation of solid and liquid surfaces. J. of L. 30:446–471 H. M. van Driel, (1985).

28. K. M. and J. Kiuchi. F. nanostruc?ture formed on hard thin films of T. and DLC. A. P. A. M. S. & P. 76:983–985 N. Yasumaru, (2003).

29. X. Li and Y. Guan, Nami Jishu Yu Jingmi Gongcheng/Nanotechnology and Precision Engineering **3**, 105 (2020).

30. J. Y. B. Z. M. W. and X. Zhu. C. of periodic ripples growth on metals by femtosecond laser ellipticity. O. E. 20:25826– 25833 Y. Tang, (2012).

31. W. C. Shen, C. W. Cheng, M. C. Yang, Y. Kozawa, and S. Sato, Journal of Laser Micro Nanoengineering **5**, 229 (2010).

32. M. F. B. and R. M. W. Y. Jee, Duced Damage on Single-Crystal Metal Surfaces. Journal of the Optical Society of America B, 5:648– 659, 1988 (n.d.).

33. E. M. Hsu, T. H. R. Crawford, C. Maunders, G. A. Botton, and H. K. Haugen, Applied Physics Letters **92**, (2008).

34. T. Tomita, R. Kumai, S. Matsuo, S. Hashimoto, and M. Yamaguchi, Applied Physics A: Materials Science and Processing **97**, 271 (2009).

35. O. Aktas and A. C. Peacock, Advanced Photonics Research **2**, 2000159 (2021).

36. J. F. Young, J. S. Preston, H. M. van Driel, and J. E. Sipe, Physical Review B **27**, 1155 (1983).

37. J. Bonse, M. Munz, and H. Sturm, Journal of Applied Physics **97**, (2005).

38. A. Borowiec and H. K. Haugen, Applied Physics Letters **82**, 4462 (2003).

39. J. Bonse, J. M. Wrobel, J. Krüger, and W. Kautek, Applied Physics A: Materials Science and Processing **72**, 89 (2001).

40. D. Milovanović, B. Rajčić, S. Petronić, A. Radulović, B. Radak, B. Gaković, M. Zamfirescu, C. Albu, and J. Savović, European Physical Journal D **76**, (2022).

41. M. Huang, F. Zhao, Y. Cheng, N. Xu, and Z. Xu, ACS Nano **3**, 4062 (2009).

42. M. Deb, E. Popova, M. Hehn, N. Keller, S. Petit-Watelot, M. Bargheer, S. Mangin, and G. Malinowski, Physical Review Letters **123**, (2019).

43. M. G. and H. F. A. J. Huis in ’t Veld, On the Origin, Growth and Application of Ripples. Journal of Laser Micro/Nanoengineering (2008).

44. J. Bonse and J. Krüger, Journal of Applied Physics **108**, (2010).

45. J. Bonse, J. M. Wrobel, J. Krüger, and W. Kautek, Applied Physics A: Materials Science and Processing **72**, 89 (2001).

46. T. Tomita, R. Kumai, S. Matsuo, S. Hashimoto, and M. Yamaguchi, Applied Physics A: Materials Science and Processing **97**, 271 (2009).

47. J. F. Young, J. E. Sipe, J. S. Preston, and H. M. van Driel, Applied Physics Letters **41**, 261 (1982).

48. H. M. van Driel, J. E. Sipe, and J. F. Young, Physical Review Letters **49**, 1955 (1982).

49. A. Y. Vorobyev, V. S. Makin, and C. Guo, Journal of Applied Physics **101**, (2007).

50. M. Deb, E. Popova, M. Hehn, N. Keller, S. Petit-Watelot, M. Bargheer, S. Mangin, and G. Malinowski, Physical Review Letters **123**, (2019).

51. M. Shiraishi, S. Kubodera, and K. Watanabe, Optical Sensors 2017 **10231**, 102311H (2017).

52. A. Borowiec and H. K. Haugen, Applied Physics Letters **82**, 4462 (2003).

53. M. Couillard, A. Borowiec, H. K. Haugen, J. S. Preston, E. M. Griswold, and G. A. Botton, Journal of Applied Physics **101**, (2007).

54. F. C. M. H. and S. V. P. J. Reif, Ripples Revisited: Non?Classical Morphology at the Bottom of Femtosecond Laser Ablation Craters in Transparent Dielectrics. Applied Surface Science, 197-198:891–895 (2002).

55. M. Groenendijk and J. Meijer, 24th International Congress on Applications of Lasers and Electro-Optics, ICALEO 2005 - Congress Proceedings 219 (2005).

56. M. Deb, E. Popova, M. Hehn, N. Keller, S. Petit-Watelot, M. Bargheer, S. Mangin, and G. Malinowski, Physical Review Letters **123**, (2019).

57. S. Shaikh, S. Kedia, D. Singh, M. Subramanian, and S. Sinha, Journal of Laser Applications **31**, 022011 (2019).

58. D. Dufft, A. Rosenfeld, S. K. Das, R. Grunwald, and J. Bonse, Journal of Applied Physics **105**, (2009).

59. K. M. and J. K. N. Yasumaru, Femtosecond-Laser-Induced Nanostruc?Ture Formed on Hard Thin Films of TiN and DLC. Applied Physics A: Materials Science & Processing, 76:983–985 (2003).

60. S. K.-A. and J. R. F. Costache, Sub-Damage-Threshold Fem?Tosecond Laser Ablation from Crystalline Si: Surface Nanostructures and Phase Transformation. Applied Physics A: Materials Science & Processing, 79:1429– 1432 (2004).

61. C. v. Raman and K. S. Krishnan, Nature **121**, 501 (1928).

62. C. Lima, H. Muhamadali, and R. Goodacre, Annual Review of Analytical Chemistry **14**, 323 (2021).

63. D. Cialla-May, M. Schmitt, and J. Popp, Physical Sciences Reviews **4**, (2019).

64. Components of a Raman Spectrometer - B&W Tek (n.d.).

65. E. & F. | B. Beer's law | Definition, (n.d.).

66. A. Downes and A. Elfick, Sensors **10**, 1871 (2010).

67. P. and F. S.-C. L. 4.5: Photoluminescence, (n.d.).

68. Vallikkodi Mahalingam, SYNTHESIS, GROWTH AND CHARACTERIZATION OF PIPERAZINIUM p-AMINOBENZOATE AND PIPERAZINIUM p-CHLOROBENZOATE NONLINEAR OPTICAL SINGLE CRYSTALS (2018).

69. 10.6: Photoluminescence Spectroscopy - Chemistry LibreTexts, (n.d.).

70. Scanning Electron Microscopy (SEM): A Review, (n.d.).

71. S. E. M. (SEM) Integrating Research and Education, (n.d.).

72. Naresh Marturi, Vision and Visual Servoing for Nanomanipulation and Nanocharacterization in Scanning Electron Microscope (2013).

73. Scanning Electron Microscope (SEM)- Definition, Principle, Parts, Images - Microbe Notes (n.d.).

74. Y. Wang, C. Cong, W. Yang, J. Shang, N. Peimyoo, Y. Chen, J. Kang, J. Wang, W. Huang, and T. Yu, Nano Research **8**, 2562 (2015).